Pan-cancer investigation reveals mechanistic insights of planar cell polarity gene *Fuz* in carcinogenesis

Zhefan Stephen Chen[1,2,*], Xiao Lin[2,*], Ting-Fung Chan[2,3], Ho Yin Edwin Chan[1,2,3]

[1]Nexus of Rare Neurodegenerative Diseases, School of Life Sciences, Faculty of Science, The Chinese University of Hong Kong, Shatin, N.T., Hong Kong SAR, China
[2]School of Life Sciences, Faculty of Science, The Chinese University of Hong Kong, Shatin, N.T., Hong Kong SAR, China
[3]Gerald Choa Neuroscience Centre, The Chinese University of Hong Kong, Shatin, N.T., Hong Kong SAR, China
*Equal contribution

Correspondence to: Zhefan Stephen Chen, Ho Yin Edwin Chan; email: b140892@cuhk.edu.hk, hyechan@cuhk.edu.hk

ABSTRACT

The fuzzy planar cell polarity protein (Fuz) is an effector component of the planar cell polarity (PCP) signaling. Together with other core and effector proteins, the PCP pathway controls polarized cell movements. Fuz was also reported as a negative regulator of cell survival. In this study, we performed a pan-cancer survey to demonstrate the role of Fuz in multiple types of cancer. In head-neck squamous cell carcinoma and lung adenocarcinoma tumor samples, a reduction of *Fuz* transcript expression was detected. This coincides with the poor overall survival probabilities of these patients. We further showed that *Fuz* promoter hypermethylation contributes to its transcriptional downregulation. Meanwhile, we also identified a relatively higher mutation frequency at the 404th arginine amino acid residue in the coding sequence of *Fuz* locus, and further demonstrated that mutant Fuz proteins perturb the pro-apoptotic function of Fuz. In summary, our study unveiled an intriguing relationship between *Fuz* dysregulation and cancer prognosis, and further provides mechanistic insights of Fuz's involvement in carcinogenesis.

INTRODUCTION

The planar cell polarity (PCP) pathway is an evolutionarily conserved signaling axis that organizes the polarized movements of cells within a planar plane to achieve tissue patterning and morphogenesis [1]. Initial studies on the molecular functions of PCP pathway emphasize the relationship between PCP signaling and mammalian embryonic development, as exemplified by the fact that genetic alterations in PCP genes lead to severe neurodevelopmental deficits [2–4]. In addition to developmental defects, the PCP pathway also takes part in human disorders, including Alzheimer's disease [1] and cancer [5, 6].

Two subsets of genes, including PCP core and effector genes, contribute to the signal transduction of the PCP pathway [7]. It is generally accepted that PCP effectors function genetically downstream of PCP core genes [8]. However, a few studies also indicate that the cellular functions of PCP core proteins could be reversely influenced by the PCP effectors, suggesting a more complex regulatory network between PCP core and effector genes in PCP signaling [9–11]. Cancer describes a broad range of diseases characterized by sustained cell proliferation and metastasis triggered by cell invasion to nearby tissues and organs [12, 13]. Several key signaling pathways, including those essential for embryonic neurodevelopment, are reported

to function during tumorigenesis as well [14–16]. This indicates that some molecular mechanisms in human neurological disorders and cancer could be mutually inclusive. Recent research further unveiled the role of PCP signaling in cancer malignancy [17] and cancer cell dissemination [18, 19]. Moreover, upregulation of PCP core gene expression, *Prickle1* and *Vangl2*, inhibits neuroblastoma cell overproliferation, and corresponds to better survival probabilities in cancer patients [20].

Fuzzy planar cell polarity protein (Fuz) is categorized as a PCP effector. Similar to the other PCP core and effector players, the molecular function of Fuz was initially studied in mammalian embryonic development. The *Fuz* knockout (*Fuz$^{-/-}$*) mice showed severe developmental retardation accompanied by the impairments in ciliogenesis and several essential developmental pathways, in particular, the Hedgehog signaling axis [10, 21]. At the cellular level, Fuz protein localizes to the basal body and ciliary axoneme to support cilia outgrowth [11]. Meanwhile, Fuz interacts to mediate the ciliary trafficking of Dishevelled (Dvl) protein, an intermediator responsible for signal transduction in Wnt pathways, suggesting a potential function of Fuz in Wnt signaling [11]. As observed in the embryonic fibroblasts isolated from *Fuz$^{-/-}$* mice, canonical Wnt/β-catenin signaling pathway was hyperactivated as demonstrated by the accumulation of nuclear β-catenin protein [11]. The expression of a group of β-catenin-targeted genes was also shown to be upregulated, which in turn causes an enhanced cell proliferation in *Fuz$^{-/-}$* mouse embryos [22]. In our previous study, we reported a novel pro-apoptotic function of the Fuz protein. When overexpressed, Fuz stimulates Dvl-Rac1-MAPK-caspase signaling cascade to trigger cell apoptosis [23]. Taken together, these findings support a crucial role of Fuz in mediating cell survival.

A previous study showed that overexpression of Fuz protein suppresses the growth of liver cancer cell line HEP1 *in vitro*, as well as in a mouse xenograft model [24]. Given the negative regulatory function of Fuz in controlling cell viability, we performed a pan-cancer survey to investigate the potential role of *Fuz* in multiple types of cancer. *Fuz* mRNA level was found downregulated in head-neck squamous cell carcinoma (HNSC) and lung adenocarcinoma (LUAD) tumor samples, and such downregulation contributes to a reduction of the overall survival probabilities in patients. Moreover, we demonstrated a tight correlation between *Fuz* transcription and *Fuz* DNA methylation level, and further showed that reduction of *Fuz* mRNA level in HNSC and LUAD tumor samples was achieved via hypermethylation of two independent CpG sites

within *Fuz* promoter region. We also identified coding sequence alterations in the *Fuz* locus across different cancer types and highlighted a relatively higher mutation frequency at 404th arginine residue. Functional analyses demonstrated that the pro-apoptotic capability of mutant Fuz protein is attenuated. In summary, this study is the first report to provide an in-depth investigation of Fuz in multiple types of cancer, and further demonstrates the effects of *Fuz* promoter DNA methylation and coding sequence alterations in cancer.

RESULTS

Investigation of prognostic value of *Fuz* in multiple cancer types

We initially used Kaplan-Meier plotter (https://kmplot.com/analysis/) to assess the prognostic significance of *Fuz* mRNA expression in 21 different types of cancer. As shown in the Kaplan-Meier curves, *Fuz* expression was found to be significantly associated with the overall survival (OS) of patients from 8 types of cancer (Figure 1). In liver hepatocellular carcinoma (LIHC) and stomach adenocarcinoma (STAD), increased *Fuz* transcript level was shown to have poor OS in patients. However, in the remaining 6 types, i.e. breast cancer (BRCA), esophageal adenocarcinoma (ESCA), head-neck squamous cell carcinoma (HNSC), kidney renal clear cell carcinoma (KIRC), kidney renal papillary cell carcinoma (KIRP) and lung adeno-carcinoma (LUAD), a reduced expression of *Fuz* was expected to contribute to decreased survival probabilities (Figure 1). The prognostic significance of *Fuz* mRNA expression was further assessed in different subtypes of breast cancer. Reduced level of *Fuz* was found to be significantly associated with poor OS in luminal A and HER2+ breast cancer patients (Supplementary Figure 1A). In addition, the prognostic significance of *Fuz* in breast cancer (Supplementary Figure 1B), lung cancer (Supplementary Figure 1C) and gastric cancer (Supplementary Figure 1D) was further supported by additional Gene Expression Omnibus (GEO) datasets.

The expression level of *Fuz*, together with other clinicopathological variables (gender, race, ethnicity, primary diagnosis, tumor stage, age at diagnosis), were analyzed and included in multivariate statistics. As summarized in Supplementary Table 1, decreased level of *Fuz* was an independent predictor of worse OS of BRCA (HR, 0.9996; 95% Cl, 0.9993-1.000; *p* value, 0.0106) and KIRP (HR, 0.9988; 95% Cl, 0.9981-1.000; *p* value, 0.00241) patients, whereas high expression of *Fuz* was independently associated with worse OS of STAD (HR, 1.001; 95% Cl, 1.0002-1.001; *p* value, 0.00257) patients.

Examination of *Fuz* transcript level in multiple cancer types

Based on our patient survival analysis (Figure 1 and Supplementary Figure 1), we next determined if *Fuz* mRNA expression was altered in primary tumor tissues. Transcriptomic profiling data mining from The Cancer Genome Atlas (TCGA) data set repository (https://portal.gdc.cancer.gov/repository) was used to evaluate *Fuz* mRNA level in all primary tumor and solid normal tissues. Moreover, paired samples, with each pair comprises tumor and adjacent non-tumor samples from the same patient, were also included to provide more convincing evaluation of *Fuz* mRNA alterations. In HNSC (Figure 2A, 2B), LUAD (Figure 2E, 2F), LIHC (Supplementary Figure 2E) and STAD (Supplementary Figure 2F), *Fuz* expression was significantly downregulated in primary tumor tissues, and such downregulation was further observed in their paired samples. Downregulation of *Fuz* in HNSC (Figure 2C, 2D), LUAD (Figure 2G) and LIHC (Supplementary Figure 3) tumor samples was further validated in additional GEO datasets. In BRCA, although *Fuz* expression was found significantly altered in primary tumor tissues, no significant alteration was identified between tumor and paired non-tumor samples (Supplementary Figure 2A). No significant change in *Fuz* expression was observed in ESCA (Supplementary Figure 2B), KIRC (Supplementary Figure 2C) and KIRP (Supplementary Figure 2D) patient samples.

In line with our survival analysis, lowered expression of *Fuz* detected in HNSC and LUAD tumor samples (Figure 2) coincides with poor OS in patients (Figure 1). We thus decided to focus on HNSC and LUAD in our subsequent studies.

Gene set enrichment analysis of genes from HNSC tumor samples with low *Fuz* expression

All primary tumor tissues with available patient survival information (n = 498) were divided into high *Fuz* expression group (n = 409) and low *Fuz* expression group (n = 89) according to the survival probabilities of HNSC patients. The low *Fuz* expression group showed poor OS in HNSC (Figure 3A). To gain further insight into the gene expression features in the low *Fuz* expression group, differential gene expression analysis was performed between low *Fuz* expression and high *Fuz* expression groups (Supplementary File 1). The log_2FC and adjusted $p < 0.001$ were used as selection criteria to determine upregulated (787 genes) and downregulated (4,748 genes) gene sets (Figure 3B). We then investigated whether these dysregulated genes are enriched in certain signaling pathways. GSEAPreranked analysis was performed to determine significantly
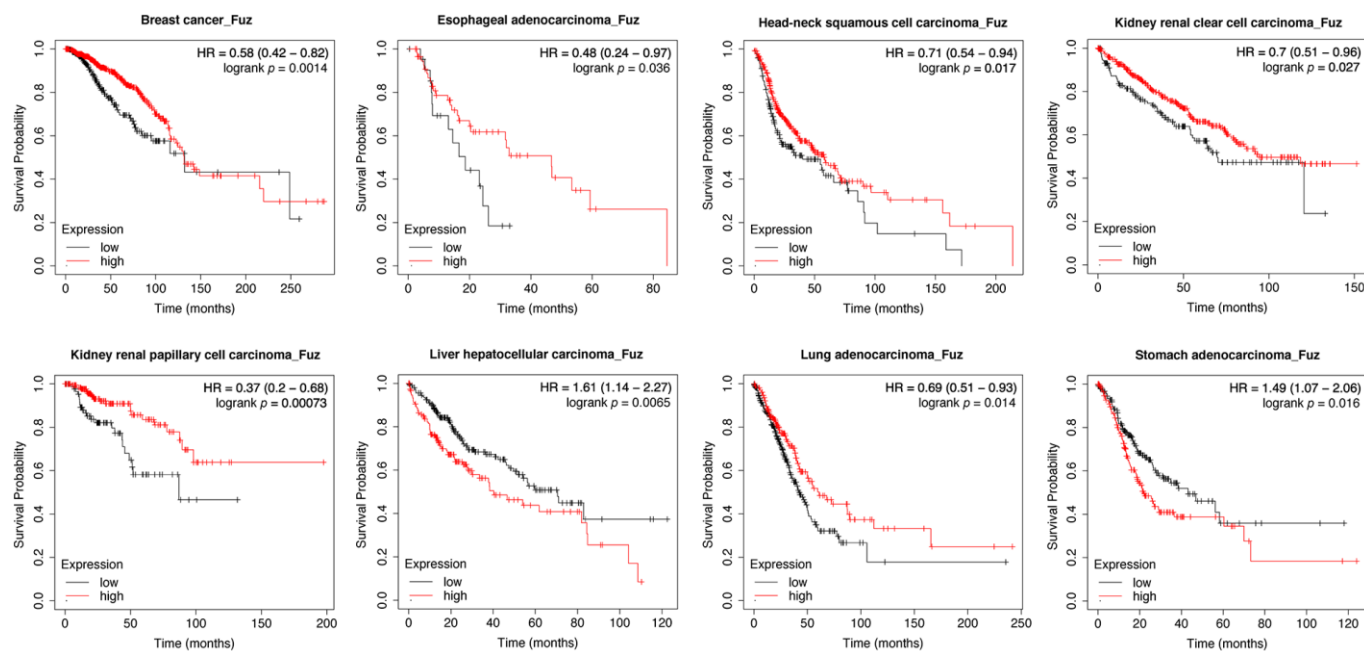

Figure 1. Evaluation of the prognostic significance of *Fuz* mRNA expression in different cancer types. Kaplan-Meier pan-cancer survival analysis was performed to evaluate the relationship between *Fuz* mRNA level and overall survival probabilities in 21 different types of cancer. Low level of *Fuz* expression was found associated with poor prognosis in BRCA, ESCA, HNSC, KIRC, KIRP and LUAD patients, whilst high level of *Fuz* expression was found associated with poor prognosis in LIHC and STAD patients.

enriched GO terms and Reactome pathways. Compared to the enriched GO terms (15 items) in the down-regulated gene set, more (26 items) were found in the upregulated gene set (Figure 3C, 3D). Meanwhile, the Reactome pathway analysis demonstrated 5 enriched downregulated pathways and 27 enriched upregulated pathways (Figure 3E, 3F). We further selected the top 500 dysregulated genes based on the $|log_2FC|$ to construct a protein-protein interaction (PPI) network by using the STRING database (https://string-db.org/). The network was visualized using Cytoscape and the densely connected MCODE network was isolated. The MCODE network was consisted of 16 genes, which were found enriched in muscle development, organization and contraction (Figure 3G).

Gene set enrichment analysis of genes from LUAD tumor samples with low *Fuz* expression

Similar to HNSC tumor samples (Figure 3A), we divided all LUAD primary tumor tissues with available patient survival information (n = 489) into high *Fuz* expression group (n = 187) and low *Fuz* expression group (n = 302). Poor OS in LUAD patients was observed in low *Fuz* expression group (Figure 4A). We then performed differential gene expression analysis between low and high *Fuz* expression groups (Supplementary File 1). The log_2FC and adjusted $p < 0.001$ were used to select upregulated (987 genes) and downregulated (2,924 genes) gene sets in the low *Fuz* expression group (Figure 4B). The ranked gene set was
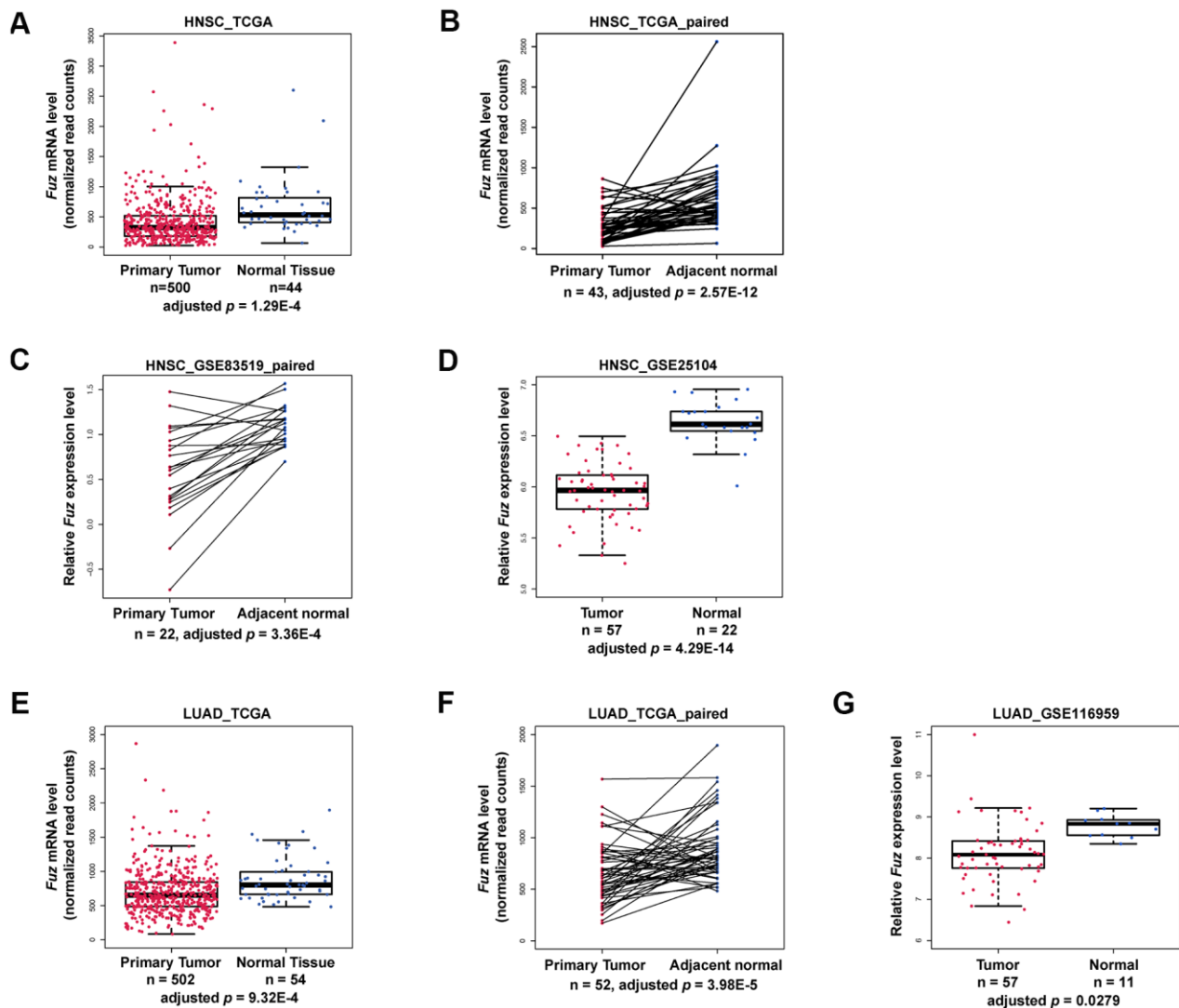

Figure 2. *Fuz* mRNA level was downregulated in HNSC and LUAD patients. (**A–D**) The expression of *Fuz* was found significantly downregulated in tumor tissues from HNSC patients. The datasets used for analysis were from TCGA, TCGA paired samples, GSE83519 and GSE25104, respectively. (**E–G**) The expression of *Fuz* was found significantly downregulated in tumor tissues from LUAD patients. The datasets used for analysis were from TCGA, TCGA paired samples and GSE116959.
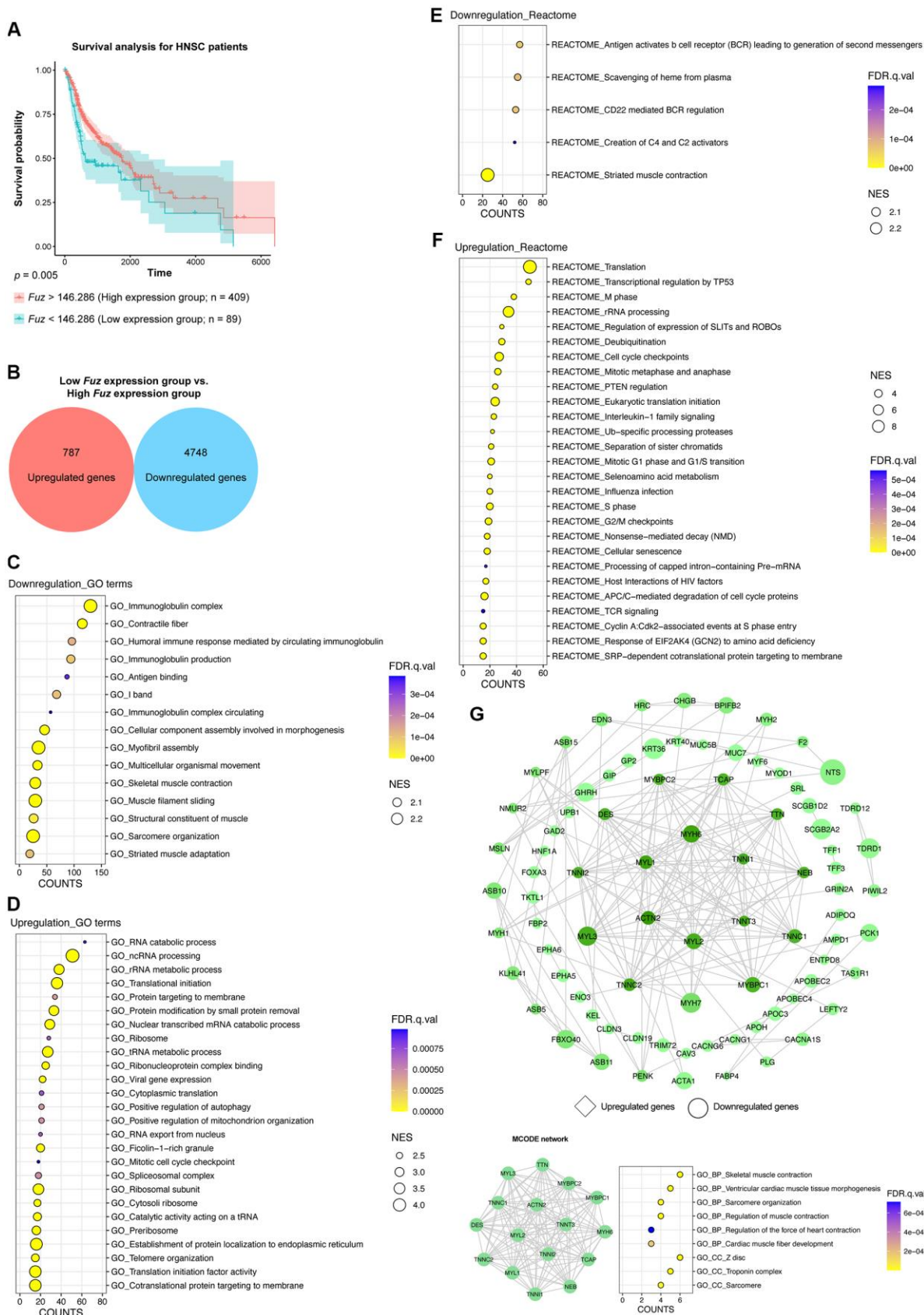
Figure 3. The gene set enrichment and PPI analyses of dysregulated genes from HNSC tumor samples with low *Fuz* expression. (**A**) The HNSC primary tumor tissues were divided into high *Fuz* expression and low *Fuz* expression groups based on the patient

survival probabilities. (**B**) The number of upregulated and downregulated genes were calculated from HNSC primary tumor tissues with low *Fuz* expression. (**C**, **D**) The GO enrichment analysis demonstrated downregulated (**C**) and upregulated (**D**) genes-associated gene ontology terms in low *Fuz* expression group. (**E**, **F**) The Reactome pathway enrichment analysis demonstrated the downregulated (**E**) and upregulated (**F**) Reactome pathways in low *Fuz* expression group. (**G**) Protein-protein interaction analysis showed the interaction between upregulated genes (in diamond shape) and downregulated genes (in circular shape) from low *Fuz* expression group. The increasing degree of nodes was indicated by continuous color (light green-dark green). The size of nodes represents fold changes of gene expression. The densely connected network was isolated using MCODE function from Cytoscape. Genes from MCODE component were annotated for GO terms with DAVID v6.8.

submitted to GSEAPreranked for the subsequent enrichment analysis. Similar to what was observed in HNSC samples, more GO terms were enriched in upregulated gene set (25 items) compared to the downregulated one (10 items) (Figure 4C, 4D). The Reactome pathway analysis identified 13 enriched upregulated pathways (Figure 4E). The top 500 dysregulated genes were selected based on the |log₂FC| for the following PPI network construction. The obtained PPI network from STRING database was visualized in Cytoscape software. The isolated MCODE network is composed of small proline-rich protein 1B (SPRR1B), small proline-rich protein 2D (SPRR2D), small proline-rich protein 2E (SPRR2E), small proline-rich protein 2F (SPRR2F) and small proline-rich protein

2G (SPRR2G), which are involved in Keratinization and Peptide cross-linking (Figure 4F).

Fuz promoter methylation is responsible for *Fuz* transcriptional downregulation in ESCA, HNSC and LUAD tumor samples

DNA methylation is one of the essential epigenetic regulators of gene expression [25]. Given that DNA methylation in gene promoter negatively controls gene transcription, we investigated whether the aberrant *Fuz* transcription is associated with alteration of *Fuz* promoter methylation in different types of cancer (Supplementary File 2). As shown in Figure 5A, 3 independent CpG methylation sites, cg11398523,
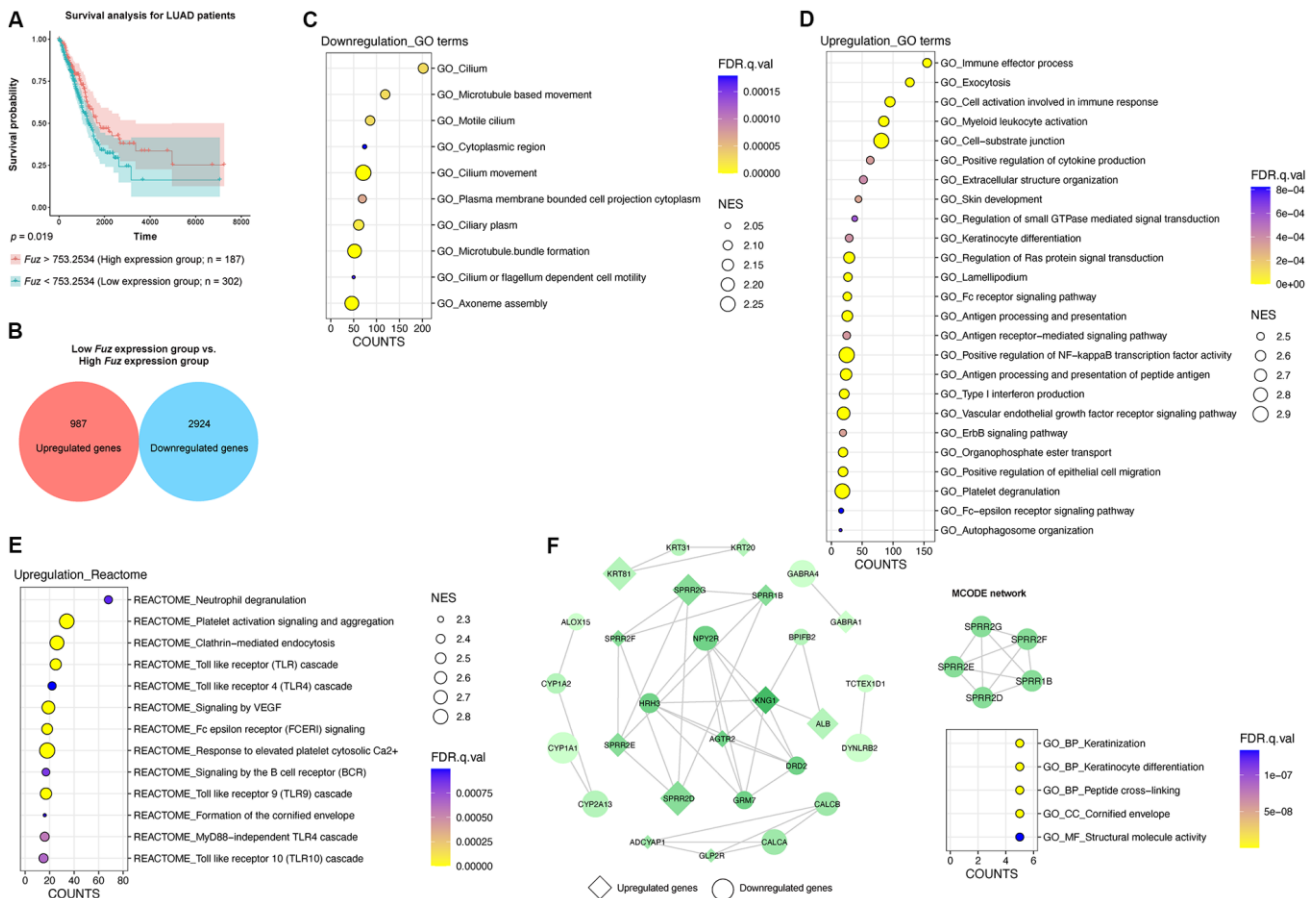

Figure 4. The gene set enrichment and PPI analyses of dysregulated genes from LUAD tumor samples with low *Fuz* expression. (**A**) The LUAD primary tumor tissues were divided into high *Fuz* expression and low *Fuz* expression groups based on the patient

survival probabilities. (**B**) The number of upregulated and downregulated genes were calculated from LUAD primary tumor tissues with low *Fuz* expression. (**C**, **D**) The GO enrichment analysis demonstrated downregulated (**C**) and upregulated (**D**) genes-associated gene ontology terms in low *Fuz* expression group. (**E**) The Reactome pathway enrichment analysis demonstrated the upregulated Reactome pathways in low *Fuz* expression group. (**F**) Protein-protein interaction analysis showed the interaction between upregulated genes (in diamond shape) and downregulated genes (in circular shape) from low *Fuz* expression group. The increasing degree of nodes was indicated by continuous color (light green-dark green). The size of nodes represents fold changes of gene expression. The densely connected network was isolated using MCODE function from Cytoscape. Genes from MCODE component were annotated for GO terms with DAVID v6.8.

cg21712019 and cg22708738, were identified within or close to a predicted CpG island in the *Fuz* promoter ($Fuz^{+117/+347CpG}$) [23]. The DNA methylation levels at sites cg11398523 and cg22708738 were found negatively associated with *Fuz* expression in multiple types of cancer, including ESCA, HNSC and LUAD (Figure 5A). The mRNA expression and DNA methylation data obtained from TCGA further confirmed an inverse correlation between *Fuz* expression and its DNA methylation level in ESCA, HNSC and LUAD primary tumor tissues (Figure 5B–5D). Moreover, upon treatment of 5-Azacytidine, inhibitor of DNA methyltransferase, *Fuz* expression was upregulated in cell lines from esophageal carcinoma (Figure 5E) and lung adenocarcinoma (Figure 5F).

We found that high *Fuz* DNA methylation at site cg11398523 and cg22708738 leads to reduced survival probabilities in HNSC and LUAD patients, respectively (Figure 6B, 6C). These coincide with our findings that lowered *Fuz* expression contributes to poor OS in HNSC and LUAD patients (Figures 3A, 4A). Meanwhile, lowered expression of *Fuz* was found associated with poor OS in ESCA patients (Supplementary Figure 4). Although a tendency of high *Fuz* DNA methylation level at site cg11398523 was observed in ESCA patients with poor OS, the difference in survival probabilities between high and low *Fuz* DNA methylation groups was not statistically significant (Figure 6A). We further compared *Fuz* DNA methylation levels between ESCA, HNSC and LUAD primary tumor tissues and their respective normal controls. As shown in Figure 6D–6F, a significant upregulation of *Fuz* DNA methylation level was detected in ESCA, HNSC and LUAD tumor samples. Taken together, these findings demonstrate a negative correlation between *Fuz* mRNA expression and *Fuz* DNA methylation level, and further suggest that *Fuz* promoter hypermethylation is a contributor to its transcriptional downregulation in ESCA, HNSC and LUAD.

Identification of *Fuz* coding sequence alterations in multiple cancer types

In addition to gene dysregulation, coding sequence alteration is another pathogenic hallmark of cancer [26]. The mutant gene product generated may confer gain- or loss-of-function and affect outputs of cancer-related pathways.

We thus explored if potential coding region variations in the *Fuz* gene exist in cancer genomes. The alteration frequency of *Fuz* was examined across 32 independent TCGA PanCancer Atlas Studies using the cBioPortal database (https://www.cbioportal.org/). Several kinds of genetic alterations, including mutation, fusion, amplification and deep deletion in the *Fuz* gene were uncovered from various cancer types, with the highest alteration frequency found in endometrial carcinoma samples (Figure 7A, Supplementary Table 2). Interestingly, a relatively higher mutation frequency at the 404th amino acid position of the Fuz protein (Fuz^{R404}) was identified (Figure 7B). The Fuz^{R404} arginine residue was found mutated in 4 tumor samples from bladder urothelial carcinoma, colorectal adenocarcinoma and uterine corpus endometrial carcinoma, and all these 4 mutated samples were caused by the single nucleotide substitution (Figure 7C). However, the missense mutation (c.G1211A) leads to a replacement of the arginine with glutamine (p.R404Q), whereas the nonsense mutation (c.C1210T) generates a truncated gene product (p.R404*; Figure 5C).

Investigation of the functional consequence of mutant Fuz protein

We previously showed a novel pro-apoptotic function of Fuz protein, however, whether mutant Fuz^{R404Q} would affect the activation of cell apoptotic pathway remains elusive. We thus examined the pro-apoptotic property of mutant Fuz protein.

The mutant Fuz expression construct harboring R404* or R404Q mutation was generated (Supplementary Figure 5). Fuz was reported to trigger cell apoptosis via activating Dvl-Rac1-MAPK-caspase-3 signaling axis [23]. We then tested the activity of this apoptotic pathway in Fuz^{R404*} or Fuz^{R404Q}-expressing cells. When overexpressed in our HEK293 cell model, the wildtype Fuz protein activates Dvl protein aggregation (from 12.22% to 50.17%), whereas such activation was attenuated in Fuz^{R404*} (27.57%) or Fuz^{R404Q} (27.18%) overexpression cells (Figure 8A, 8B). Moreover, although expressed at comparable levels, the JNK-caspase-3 activation triggered by wildtype Fuz protein was found mitigated in Fuz^{R404*} or Fuz^{R404Q}-expressing cells (Figure 8C–8F). In addition, the Fuz-mediated suppression of cell proliferation was alleviated in Fuz^{R404*} or Fuz^{R404Q} overexpression cells (Figure 8G).
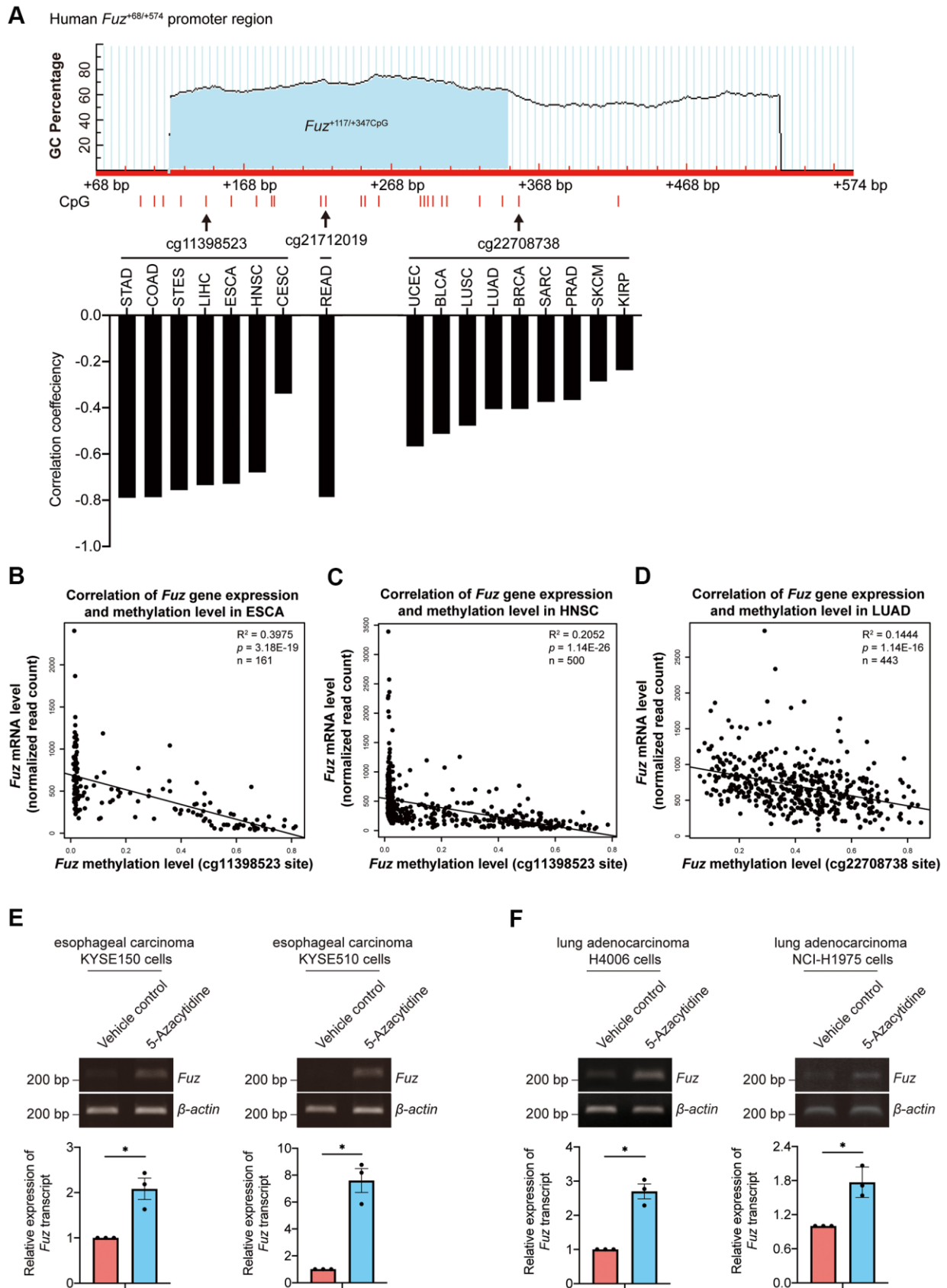
Figure 5. *Fuz* expression was associated with its promoter methylation level in ESCA and LUAD tumor samples. (**A**) *Fuz* methylation data obtained from Firebrowse database indicates that *Fuz* mRNA level was negatively associated with its promoter methylation

level in various types of cancer. Three methylation sites (cg11398523, cg21712019 and cg22708738) were highlighted, and these sites reside within or close to a potential CpG island ($Fuz^{+117/+347CpG}$) in $Fuz^{+68/+574}$ promoter region. The CpG island $Fuz^{+117/+347CpG}$ was predicted using MethPrimer software (https://www.urogene.org/cgi-bin/methprimer/methprimer.cgi) [27]. (**B**, **C**) *Fuz* mRNA level negatively correlates with the methylation at cg11398523 site within *Fuz* promoter in ESCA (**B**) and HNSC (**C**) patient samples. (**D**) A negative correlation between *Fuz* expression and *Fuz* promoter methylation level (at cg22708738 site) was identified in LUAD patient samples. (**E**) Treatment of 5-Azacytidine upregulated *Fuz* transcript level in esophageal carcinoma KYSE150 and KYSE510 cell lines. (**F**) *Fuz* transcript level was increased upon treatment of 5-Azacytidine in lung adenocarcinoma H4006 and NCI-H1975 cell lines. n = 3 biological replicates. Each n represents an independent preparation of cell RNA samples. Error bars represent S.E.M. Statistical analysis was performed using two-tailed unpaired Student's t-test. * denotes $p < 0.05$.

DISCUSSION

Fuz is one of the PCP effectors that have been implicated in governing mammalian embryonic development [10, 21]. In addition to Fuz, Inturned and WDPCP are the other two PCP effector players. Unlike Inturned and WDPCP, which have been linked to different types of cancer [28–30], the study of Fuz in cancer remains under-investigated. In the current study, we uncovered that *Fuz* expression associates with patient survival probabilities in 8 types of cancer (Figure 1). In HNSC and LUAD, *Fuz* expression is reduced (Figure 2), and such reduction correlates with the poor survival probabilities in patients (Figures 3A, 4A).
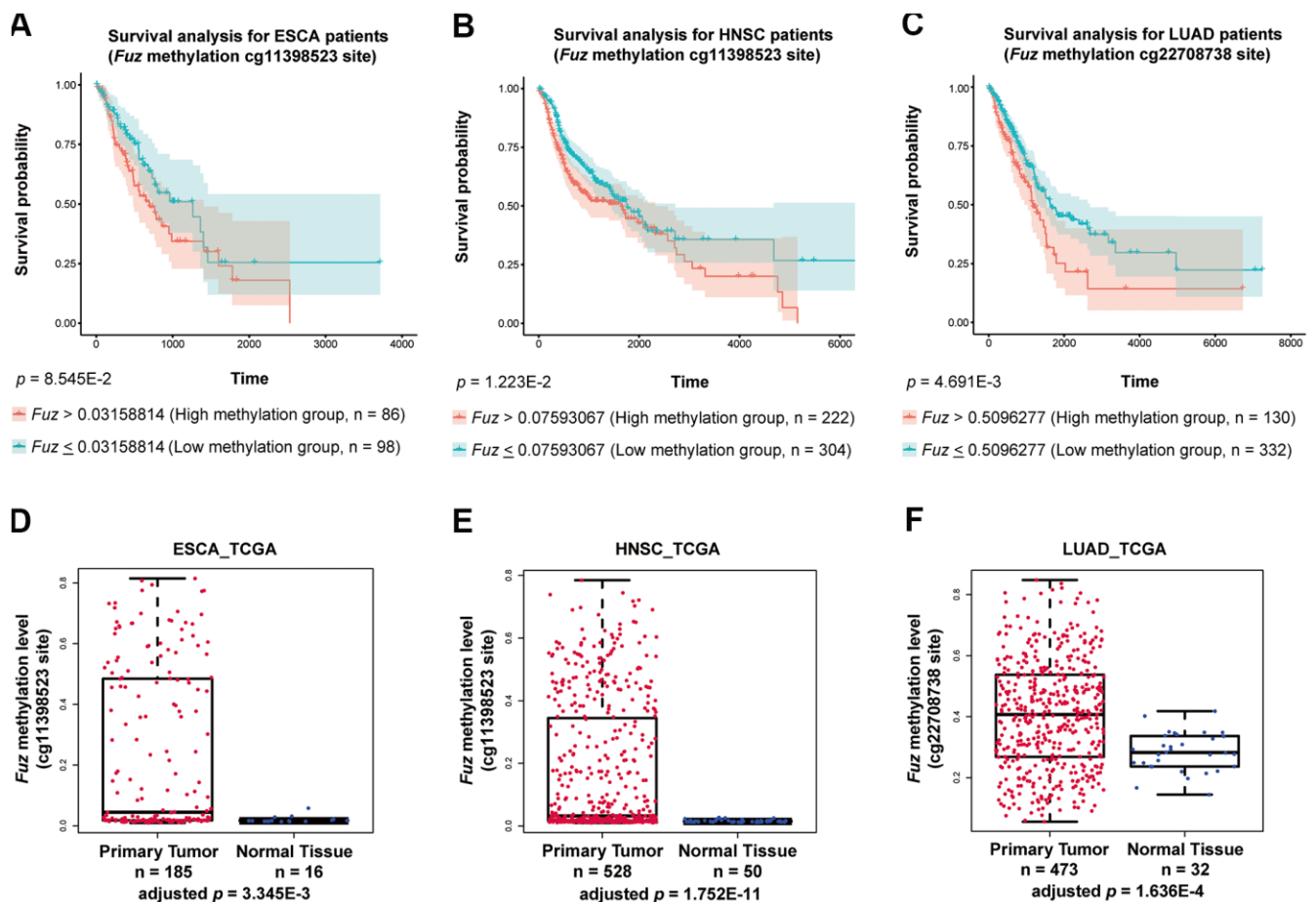

Figure 6. High methylation of *Fuz* promoter associated with poor survival probabilities in HNSC and LUAD patients, and *Fuz* promoter methylation level was significantly upregulated in tumor samples from ESCA, HNSC and LUAD patients. (**A**) Difference in *Fuz* promoter methylation level did not cause a significant alteration of survival probability in ESCA patients. (**B**, **C**) High *Fuz* promoter methylation leads to poor overall survival in HNSC (**B**) and LUAD (**C**) patients. (**D**, **E**) The methylation level of *Fuz* at cg11398523 site was significantly upregulated in ESCA (**D**) and HNSC (**E**) patient tumor samples. (**F**) The methylation level of *Fuz* at cg22708738 site was significantly upregulated in LUAD patient tumor samples.

Interestingly, physical interactions have been demonstrated among PCP effectors, and their subcellular localization can be mutually modulated in *Drosophila* wing cells [9, 31]. Further investigations to consider Fuz, Inturned and WDPCP as a functional

group could unveil more pathogenic details of PCP effectors in cancer.

Head and neck cancer and lung cancer are both the leading causes of cancer-associated mortality world-
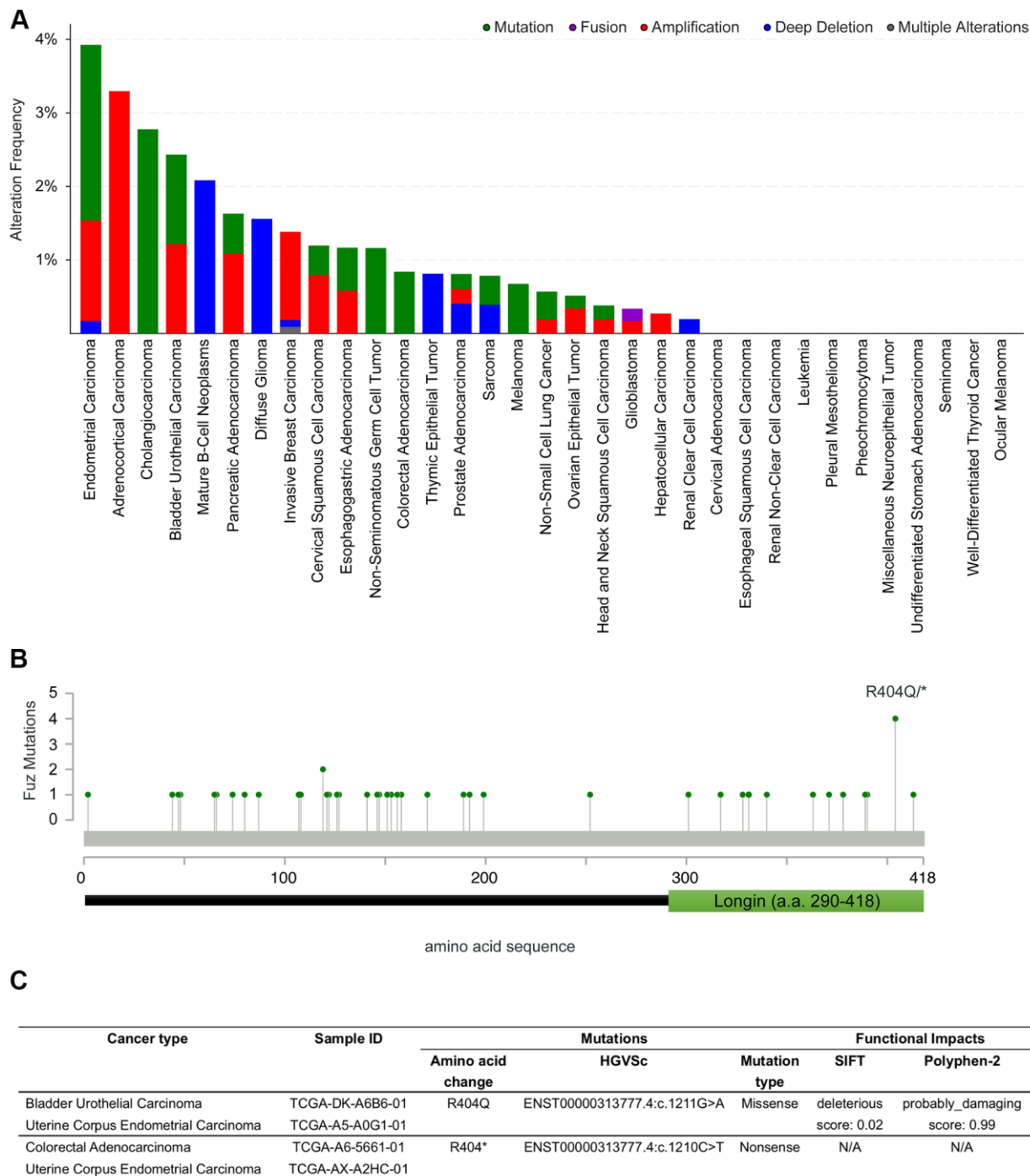

Figure 7. Coding sequence alterations in *Fuz* were identified across multiple cancer types. (A) cBioportal online database was used to investigate *Fuz* coding sequence alterations in multiples types of cancer. (B) A relative higher mutation frequency was identified at the 404th arginine residue within the coding sequence at *Fuz* locus. (C) The missense and nonsense mutations at Fuz[R404] were identified in 4 patient samples from 3 independent studies.
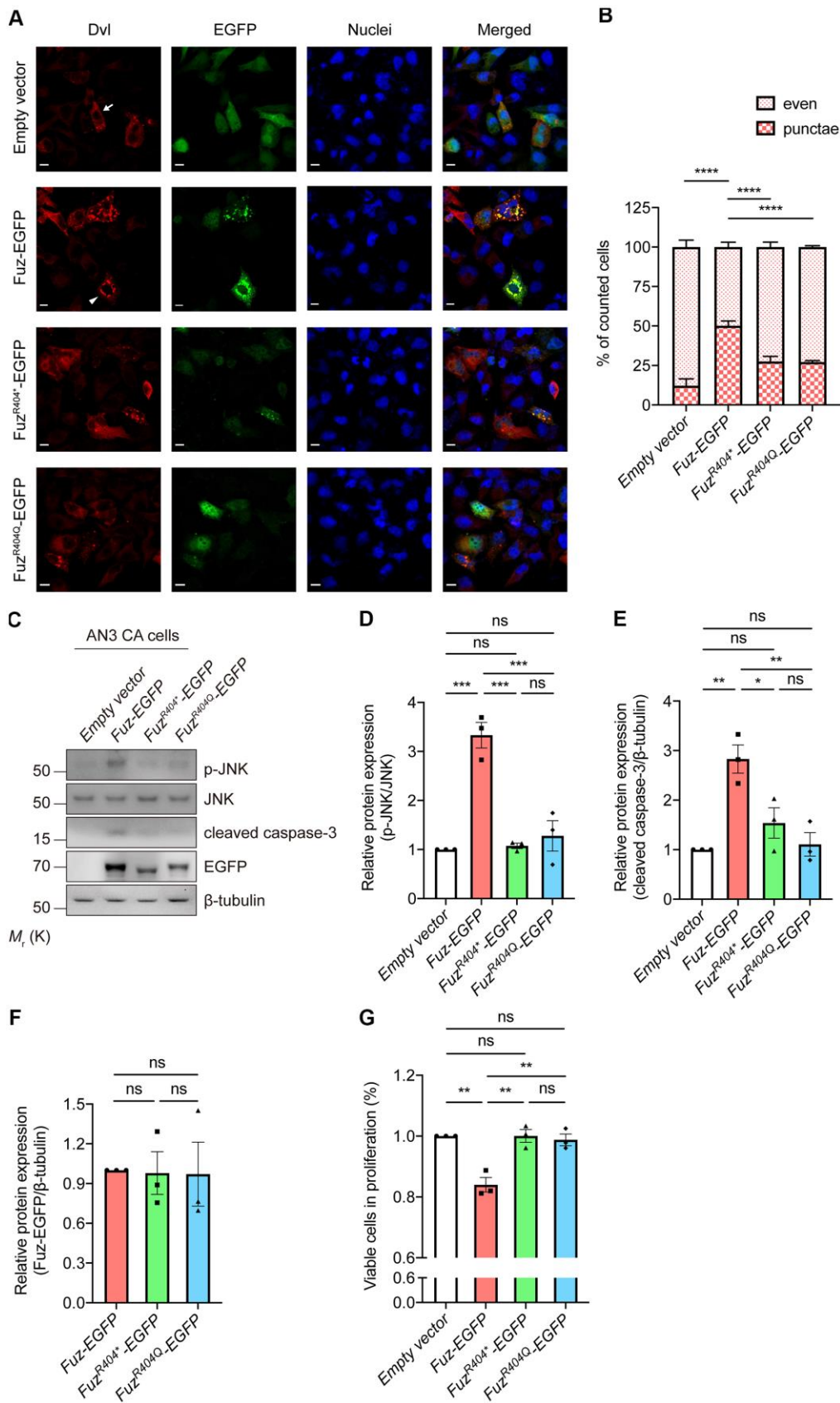
Figure 8. Overexpression of mutant Fuz proteins did not lead to the activation of cell apoptotic pathway. (**A**) When solely expressed in HEK293 cells, Dvl protein (red) showed two distinct staining patterns, which consist evenly distributed Dvl (arrow) and punctate

Dvl (arrowhead). The evenly distributed Dvl is the predominant staining pattern. Overexpression of Fuz (green) promoted the formation of Dvl punctae, while such effect was attenuated in Fuz[R404*] or Fuz[R404Q]-expressing cells. Cell nuclei (blue) were stained with Hoechst 33342. Scale bars: 10 µm. n = 3 biological replicates. Each n represents an independent preparation of immunocytochemistry sample. At least 100 cells were counted in each control or experimental group from an independent experiment. (**B**) is the quantification of (**A**). Error bars represent S.E.M. Statistical analysis was performed using one-way ANOVA followed by *post hoc* Tukey's test. **** denotes $p < 0.0001$. (**C**) Overexpression of Fuz, but not Fuz[R404*] or Fuz[R404Q], promoted JNK-caspase-3 activation in HEK293 cells. n = 3 biological replicates. Each n represents an independent preparation of cell protein samples. (**D–F**) Quantification of p-JNK, cleaved caspase-3 and Fuz-EGFP protein expression in (**C**). Error bars represent S.E.M. Statistical analysis was performed using one-way ANOVA followed by *post hoc* Tukey's test. ns denotes no significant difference, * denotes $p < 0.05$, ** denotes $p < 0.01$ and *** denotes $p < 0.001$. (**G**) Overexpression of Fuz, but not Fuz[R404*] or Fuz[R404Q], suppressed the percentage of viable cells in proliferation. n = 3 biological replicates. Each n represents an independent preparation of cell proliferation assay samples. Error bars represent S.E.M. Statistical analysis was performed using one-way ANOVA followed by *post hoc* Tukey's test. ns denotes no significant difference, ** denotes $p < 0.01$.

wide [32, 33]. As one of the key pathogenic features, gene dysregulation leads to dysfunctions of essential signaling pathways, which in turn contribute to cancer development and progression [34]. In this study, a GSEA approach was exploited to investigate enriched gene functions and pathways in HNSC and LUAD patients with poor OS (Figures 3, 4). In HNSC, the genes related to muscle contraction and immuno-globulin production and circulation were down-regulated, whereas the upregulated genes were enriched in RNA processing and protein synthesis and modification (Figure 3C, 3D). Meanwhile, the Reactome pathway analysis highlights the enrichment of several cancer-related pathways, including mitotic metaphase and anaphase [35], cell cycle checkpoints [36] and transcriptional regulation by TP53 [37] (Figure 3F). Pharmacological inhibition of key factors related to cell cycle regulation, such as WEE1 G2 checkpoint kinase and checkpoint kinase 1, has been shown to force the HNSC cells skipping the cell cycle checkpoints, leading to accumulation of massive DNA damage and eventually cell death [38, 39]. Somatic mutation in TP53 is one of the most frequent genetic alterations among human cancers, including HNSC [40]. The variable TP53 mutational landscape in HNSC bears distinct activities of downstream pathological pathways, and mutant p53 dysregulates a range of oncogenic molecules in favor of malignant phenotype in HNSC cells [41–43]. In line with previous reports, our findings further emphasize the importance of cell cycle regulation and TP53 signaling in HNSC. In LUAD, the upregulated genes were enriched in immune response and exocytosis (Figure 4D). The Reactome pathway enrichment results further point out upregulation of several toll like receptor cascades, which are crucial for executing innate immune response (Figure 4E). Meanwhile, genes focusing on cilium organization were downregulated (Figure 4C). Interestingly, the histological examination of lung tumor samples reveals loss of ciliary structures, and the cilia-related gene expression was found markedly decreased [44, 45]. Moreover, stimulation of ciliogenesis combats against invasion, cell proliferation and epithelial-mesenchymal transition of lung cancer cells [46]. Given the role of

PCP signaling in mediating ciliogenesis, our study further suggests the pathological significance of cilia biogenesis in LUAD.

Fuz transcription negatively correlates with its promoter DNA methylation level. When the human embryonic 293 cells are treated with 5-Azacytidine, a DNA methyltransferase inhibitor, *Fuz* mRNA level is found upregulated [23]. In our previous study, a putative CpG island within *Fuz* promoter, $Fuz^{+117/+347CpG}$, was identified. We further reported that a transcriptional factor, YY1, maintains the methylation of $Fuz^{+117/+347CpG}$ to achieve the transcriptional repression of *Fuz* expression [23]. In this study, we further showed that DNA methylation of three independent CpG sites negatively correlates with *Fuz* mRNA level (Figure 5A). All these three CpG sites reside within or close to $Fuz^{+117/+347CpG}$, and two of them were found negatively associated with *Fuz* expression in various cancer types, including ESCA, HNSC and LUAD (Figure 5B–5D). Such association was further validated by experimental evidence. When the esophageal carcinoma and lung adenocarcinoma cells were treated with 5-Azacytidine, *Fuz* transcription was upregulated (Figure 5E, 5F). In 2017, Hao et al. [24] demonstrated a negative correlation between *Fuz* expression and its promoter DNA methylation level in LIHC tumor samples at another CpG site, cg19763319, which is also close to the $Fuz^{+117/+347CpG}$ region. These findings highlight $Fuz^{+117/+347CpG}$ as a core regulatory element in governing *Fuz* transcription. Any possible dysregulation of the $Fuz^{+117/+347CpG}$ methylation level may contribute to the pathogenesis of human diseases, including cancer.

In this study, we also determined the functional consequence of mutant Fuz proteins, Fuz[R404*] and Fuz[R404Q]. The mutation at Fuz[R404] residue resides within a predicted Longin domain (a.a. 290-418) in the Fuz protein C-terminus [21, 31, 47]. When overexpressed in cells, the wildtype Fuz protein triggers cell apoptosis via activating Dvl-Rac1-MAPK-caspase signaling cascade [23]. However, such activation was found attenuated in Fuz[R404*] or Fuz[R404Q]-expressing cells, suggesting the deterioration of Fuz pro-apoptotic

function (Figure 8). Since Fuz^{R404*} and Fuz^{R404Q} mutations were identified in cancer patient samples, this functional evidence may provide more clues on how the perturbation of Fuz protein functions leads to the cell overproliferation in certain types of cancer.

Both R404* and R404Q mutations occur in the highly conserved 404th arginine residue within the Fuz Longin domain [47]. The presence of Longin domain is broadly shared by vesicle trafficking proteins [48, 49]. These Longin domain-containing proteins transport specific cargos and target their membrane localization in support of cilia outgrowth, which is impaired when protein dysfunctions occur [11, 50]. Interestingly, the R404Q mutation was initially identified from human patients with neural tube defects, a severe neurological deficit due to the failure of neural tube closure during embryonic development, and Seo et al. [47] showed that Fuz^{R404Q} mutant prevents cilia elongation and directional cell movements. Taken together, these findings suggest the importance of Longin domain in carrying out Fuz biological function, especially in regulating ciliogenesis. In our functional experiments, we found that, both Fuz^{R404*} and Fuz^{R404Q} mutants alleviated the stimulation of cell apoptosis (Figure 8). It would therefore be intriguing to further investigate the functional significance of Longin domain with respect to the pro-apoptotic activity of Fuz protein.

In conclusion, our study is the first report to demonstrate the mechanistic insights of a PCP effector, *Fuz*, in multiple types of cancer. The development of interventions targeting *Fuz* DNA methylation alteration and coding sequence mutations may be therapeutically beneficial towards carcinogenesis.

MATERIALS AND METHODS

Kaplan-Meier plotter analysis

The pan-cancer survey from the online database Kaplan-Meier Plotter (https://kmplot.com/analysis/index.php?p=service&cancer=pancancer_rnaseq) was used to evaluate the prognostic value of *Fuz* mRNA expression in 21 different types of cancer [51]. In particular, the prognostic value of *Fuz* mRNA expression in different breast cancer subtypes was analyzed separately (https://kmplot.com/analysis/index.php?p=service&cancer=breast). Moreover, the prognostic value of *Fuz* mRNA expression in additional Gene Expression Omnibus datasets of breast cancer (https://kmplot.com/analysis/index.php?p=service&cancer=breast), lung cancer (https://kmplot.com/analysis/index.php?p=service&cancer=lung) and gastric cancer (https://kmplot.com/analysis/index.php?p=service&cancer=gastric) was also assessed using Kaplan-Meier

Plotter. The patient samples were split into two groups (high expression *vs*. low expression) based on the auto selected best cutoff for *Fuz* expression. The overall survival probability of cancer patients was assessed using the Kaplan-Meier survival plots, and logrank *p* value was calculated to determine whether the association between *Fuz* expression and patient survival is statistically significant.

Processing of TCGA data

The RNA sequencing data and DNA methylation data of primary tumor tissues and solid normal tissues were obtained from The Cancer Genome Atlas (TCGA) Research Network (https://www.cancer.gov/tcga) via the GDC Data Portal (https://portal.gdc.cancer.gov/) [52] on June 27, 2018. The raw gene expression counts generated by HTSeq [53] were imported to DESeq2 (1.24.0) [54] in R (v3.6.3) for normalization and the normalized gene counts were used for downstream analysis. DESeq2 was used to perform the differential gene expression analysis, and standard DESeq2 Wald test, followed by the Benjamini-Hochberg correction was used for multiple comparisons. Wilcoxon Rank Sum test followed by Benjamini-Hochberg correction was used to compare methylation levels between tumor and normal tissues. To determine the correlation between *Fuz* mRNA level and *Fuz* DNA methylation level, the normalized gene counts were regressed on the DNA methylation levels using linear model with the function 'lm' in R. The Cox regression was performed using the 'survival' (3.2.7) and 'survminer' (0.4.7) packages in R to determine the association between *Fuz* DNA methylation level and patient survival probabilities. Multivariate survival analysis was performed again, with 'survival' and survminer', using the seven factors retrieved from the TCGA clinical data, including gender, race, ethnicity, primary_diagnosis, tumor stage and age at diagnosis. In addition, the normalized expression level of *Fuz* was also included.

Gene set enrichment analysis (GSEA)

The gene enrichment analysis was carried out using GSEA v4.0.3 software (https://www.gsea-msigdb.org/gsea/index.jsp) [55]. The gene ranks were generated by using DESeq2 to calculate fold changes of normalized gene counts between low *Fuz* and high *Fuz* expression groups in HNSC and LUAD tumor samples (Supplementary File 1). The annotated gene sets c5.go.v7.2.symbols.gmt was used for the Gene Ontology (GO) terms enrichment analysis, while the annotated gene set c2.cp.reactome.v7.2.symbols.gmt was used for the Reactome pathways enrichment analysis. The GSEAPreranked analysis was performed with the number of permutations set as 1,000 times for

each analysis. The selection criteria for significantly enriched GO terms and Reactome pathways were |normalized enrichment score (NES)| > 2 and false discovery rate (FDR) q-value < 0.001.

Protein-protein interaction (PPI) network analysis

The PPI network analysis was performed using STRING v11.0 database (https://string-db.org/) [56]. The protein-protein interaction network was constructed based on experimental evidence, computational predictions and co-expression networks. Top 500 dysregulated genes selected based on |log$_2$FC| from low *Fuz* expression groups were used as input, and the minimum required interaction score was defined as highest confidence (0.900) to carry out the prediction. The Cytoscape v3.8.0 was used to visualize the constructed PPI network, and Molecular Complex Detection (MCODE) algorithm was used to select densely connected networks. The significantly (FDR < 0.001) enriched GO terms in the MCODE networks were isolated from DAVID 6.8 database (https://david.ncifcrf.gov/home.jsp) [57].

cBioPortal analysis

cBioPortal v3.3.5 is a comprehensive web resource to provide visualization and analysis of cancer genomic data (https://www.cbioportal.org/) [58]. The genomic alteration profiles in *Fuz*, including mutations and copy number alterations, were obtained from 10,967 samples of 32 independent TCGA PanCancer Atlas Studies.

Molecular cloning

The *pcDNA3.1 (zeo)-flag-Dvl* was a kind gift from Prof. Randall Moon (Addgene plasmid # 16758). The *Fuz-EGFP* was described previously [23]. The *Fuz^{R404*}* DNA sequence was amplified from *Fuz-EGFP* using primers *EcoRI-Fuz-F*, 5`-CCGGAATTCATGGGGGA GGAGGGGAC-3` and *KpnI-Fuz$^{R404\ stop}$-R*, 5`-CCGGGTACCGTTCACAGCCCATGGGTG-3`. The resultant DNA fragment was subcloned into *pEGFP-N1* (Clontech Laboratories) expression vector using *Eco*RI and *Kpn*I to generate *Fuz^{R404*}-EGFP* mutant construct. Overlapping PCR method was used to generate the *Fuz^{R404Q}* mutant sequence, the resultant DNA fragment was subcloned into *pEGFP-N1* expression vector using *Eco*RI and *Kpn*I to generate *Fuz^{R404Q}-EGFP* mutant construct. Primers used for overlapping PCR were *EcoRI-Fuz-F*, 5`-CCGGAATTCATGGGGGAGGAGG GGAC-3`, *Fuz^{R404Q}-F*, 5`- ACCCATGGGCTGCAAAG CCTGGCC-3`, *Fuz^{R404Q}-R*, 5`- GGCCAGGCTTTGCA GCCCATGGGT-3` and *KpnI-Fuz-R*, 5`- CCGGGTAC CGTAAGAAGTGGGGTGAGG-3`.

Cell culture and plasmid transfection

The human esophageal carcinoma cell lines KYSE150 and KYSE510 were kind gifts from Prof. Qian Tao (Department of Clinical Oncology, The Chinese University of Hong Kong) [59]. The human endometrial adenocarcinoma cell line AN3 CA was a kind gift from Prof. Chi Chiu Wang (Department of Obstetrics and Gynecology, The Chinese University of Hong Kong). The human lung adenocarcinoma cell lines H4006 (CRL-2871™) and NCI-H1975 (CRL-5908™) were obtained from American Type Culture Collection. All cell lines were cultured using Gibco™ RPMI 1640 Medium (21875034, Thermo Fisher Scientific) supplemented with 10% fetal bovine serum (F7524, Sigma-Aldrich) and 1% Antibiotic-Antimycotic solution (15240062, Thermo Fisher Scientific). The cells were maintained in a 37° C humidified cell culture incubator supplemented with 5% CO$_2$. Lipofectamine 2000 (11668019, Thermo Fisher Scientific) was used in plasmid transfection. The ratio between plasmid (µg) and Lipofectamine 2000 (µl) was 1:2. For immunocytochemistry samples preparation, 0.3 µg *pcDNA3.1 (zeo)-flag-Dvl*, together with 0.5 µg *EGFP-N1*, *Fuz-EGFP*, *Fuz^{R404*}-EGFP* or *Fuz^{R404Q}-EGFP*, were used for transfection. The transfection lasted for 48 h. For immunoblotting samples preparation, 1.0 µg *EGFP-N1*, *Fuz-EGFP*, *Fuz^{R404*}-EGFP* or *Fuz^{R404Q}-EGFP* was used for transfection, and the transfection lasted for 72 h. For cell proliferation assay, 0.3 µg *EGFP-N1*, *Fuz-EGFP*, *Fuz^{R404*}-EGFP* or *Fuz^{R404Q}-EGFP* was used for transfection, and the transfection lasted for 72 h.

Drug treatment

The KYSE150, KYSE510, H4006 and NCI-H1975 cells were treated with 2 µM 5-Azacytidine (0210082150, MP Biomedicals™). The treatment lasted 72 h, with medium and drug refreshed every 24 h.

Reverse transcription PCR

RNAs were extracted from cancer cell lines using the Qiagen RNeasy Mini Kit (74104, Qiagen). One microgram of RNA was used for reverse transcription using ImProm-II™ Reverse Transcription System (A3800, Promega), according to the manufacturer's instructions. Primers used in this study were *Human Fuz-119-F*, 5`-TCTCTGTCATCGGTTCCCTC-3`; *Human Fuz-366-R*, 5`-CTCCACGTTGCGGATATTG G-3`; *Actin-F*, 5`-ATGTGCAAGGCCGGTTTCGC-3`; *Actin-R*, 5`-CGACACGCAGCTCATTGTAG-3`. The PCR products were amplified using Phusion™ High-Fidelity DNA Polymerase (F530S, Thermo Fisher Scientific) and visualized on the Bio-Rad ChemiDoc imaging system.

Immunocytochemistry

The AN3 CA cells were seeded on coverslips (Marienfeld-Superior). After 48 h, cells were transfected. After another 48 h, transfected cells were fixed with 3.7% paraformaldehyde for 15 min followed by permeabilization with 0.1% Triton X-100 for another 15 min. The cells were blocked with 5% goat serum at 25° C for 1 h, followed by the incubation with primary antibody at 4° C for 16 h. The cells were then washed 3 times with 1X PBS for 5 min each. The secondary antibody was used to incubate cells at 25° C for 1 h. The cells were then washed 5 times with 1X PBS for 5 min each. The primary and secondary antibodies used were anti-flag (1:200; F3165, Sigma-Aldrich) and goat anti-mouse IgG (H+L) Cy3 conjugate (1:400; 81-6515, Zymed, Thermo Fisher Scientific). The cell nuclei were stained with Hoechst 33342 (1:400; H-1399, Thermo Fisher Scientific) at 25° C for 5 min. Cell images were acquired using a confocal microscope Zeiss LSM (Zeiss) and images were analyzed using Fiji software (Version 2.0.0-rc-69/1.52n, NIH).

Immunoblotting

The AN3 CA cells were seeded in 24-well plates (3526, Corning). After 48 h, cells were transfected. After another 72 h, transfected cells were harvested in SDS sample buffer (100 mM Tris-HCl, pH 6.8, 2% SDS, 40% glycerol, 5% β-mercaptoethanol and 0.1% bromophenol blue). Samples were heated at 99° C for 10 min prior to being subjected to the immunoblot analysis. Primary antibodies used were anti-p-JNK (1:500, 9251, Cell Signaling Technology), anti-JNK (1:1,000, 9252, Cell Signaling Technology), anti-cleaved caspase-3 (1:500; 9664, Cell Signaling Technology), anti-GFP (1:2,000; 632381, Clontech Laboratories, Inc.) and anti-β-tubulin (1:2,000; ab6046, Abcam). Secondary antibodies used for immunoblotting were HRP conjugated Goat anti-Rabbit IgG (H+L) (1:5,000, G-21234, Thermo Fisher scientific) and HRP conjugated Goat anti-Mouse IgG (H+L) (1:5,000, G-21040, Thermo Fisher Scientific). The signal was developed using Immobilon Forte Western HRP substrate (WBLUF0100, Merck Millipore) and visualized on the Bio-Rad ChemiDoc imaging system.

Cell proliferation assay

The AN3 CA cells were seeded in 96-well plates (3603, Corning). After 48 h, cells were transfected. After another 72 h, transfected cells were added with CellTiter 96® AQueous One Solution Reagent (G3582, Promega). The reaction was incubated at 37° C for 1 h, followed by the measurement of absorbance at 490 nm on a FLUOstar Omega Microplate Reader (BMG LABTECH).

AUTHOR CONTRIBUTIONS

Z.S.C. and H.Y.E.C. designed research; Z.S.C. and X.L. performed experiments and analyzed data; Z.S.C., X.L., T.F.C. and H.Y.E.C. interpreted the results and wrote the paper.

CONFLICTS OF INTEREST

The authors declare that they have no conflicts of interest.

FUNDING

REFERENCES

1. Sellers KJ, Elliott C, Jackson J, Ghosh A, Ribe E, Rojo AI, Jarosz-Griffiths HH, Watson IA, Xia W, Semenov M, Morin P, Hooper NM, Porter R, et al. Amyloid β synaptotoxicity is Wnt-PCP dependent and blocked by fasudil. Alzheimers Dement. 2018; 14:306–17.
   https://doi.org/10.1016/j.jalz.2017.09.008
   PMID:29055813

2. Torban E, Wang HJ, Groulx N, Gros P. Independent mutations in mouse Vangl2 that cause neural tube defects in looptail mice impair interaction with members of the dishevelled family. J Biol Chem. 2004; 279:52703–13.
   https://doi.org/10.1074/jbc.M408675200
   PMID:15456783

3. Yu H, Smallwood PM, Wang Y, Vidaltamayo R, Reed R, Nathans J. Frizzled 1 and frizzled 2 genes function in palate, ventricular septum and neural tube closure: general implications for tissue fusion processes. Development. 2010; 137:3707–17.
   https://doi.org/10.1242/dev.052001 PMID:20940229

4. Heydeck W, Liu A. PCP effector proteins inturned and fuzzy play nonredundant roles in the patterning but not convergent extension of mammalian neural tube. Dev Dyn. 2011; 240:1938–48.
   https://doi.org/10.1002/dvdy.22696 PMID:21761479

5. Katoh M. Wnt/PCP signaling pathway and human cancer (review). Oncol Rep. 2005; 14:1583–88.

https://doi.org/10.3892/or.14.6.1583
PMID:16273260

6. Corda G, Sala A. Non-canonical Wnt/PCP signalling in cancer: Fzd6 takes centre stage. Oncogenesis. 2017; 6:e364.
https://doi.org/10.1038/oncsis.2017.69
PMID:28737757

7. Butler MT, Wallingford JB. Planar cell polarity in development and disease. Nat Rev Mol Cell Biol. 2017; 18:375–88.
https://doi.org/10.1038/nrm.2017.11 PMID:28293032

8. Wong LL, Adler PN. Tissue polarity genes of drosophila regulate the subcellular location for prehair initiation in pupal wing cells. J Cell Biol. 1993; 123:209–21.
https://doi.org/10.1083/jcb.123.1.209 PMID:8408199

9. Wang Y, Yan J, Lee H, Lu Q, Adler PN. The proteins encoded by the drosophila planar polarity effector genes inturned, fuzzy and fritz interact physically and can re-pattern the accumulation of "upstream" planar cell polarity proteins. Dev Biol. 2014; 394:156–69.
https://doi.org/10.1016/j.ydbio.2014.07.013
PMID:25072625

10. Park TJ, Haigo SL, Wallingford JB. Ciliogenesis defects in embryos lacking inturned or fuzzy function are associated with failure of planar cell polarity and hedgehog signaling. Nat Genet. 2006; 38:303–11.
https://doi.org/10.1038/ng1753 PMID:16493421

11. Zilber Y, Babayeva S, Seo JH, Liu JJ, Mootin S, Torban E. The PCP effector fuzzy controls cilial assembly and signaling by recruiting Rab8 and dishevelled to the primary cilium. Mol Biol Cell. 2013; 24:555–65.
https://doi.org/10.1091/mbc.E12-06-0437
PMID:23303251

12. Riggi N, Aguet M, Stamenkovic I. Cancer metastasis: a reappraisal of its underlying mechanisms and their relevance to treatment. Annu Rev Pathol. 2018; 13:117–40.
https://doi.org/10.1146/annurev-pathol-020117-044127 PMID:29068753

13. Feitelson MA, Arzumanyan A, Kulathinal RJ, Blain SW, Holcombe RF, Mahajna J, Marino M, Martinez-Chantar ML, Nawroth R, Sanchez-Garcia I, Sharma D, Saxena NK, Singh N, et al. Sustained proliferation in cancer: mechanisms and novel therapeutic targets. Semin Cancer Biol. 2015; 35:S25–54.
https://doi.org/10.1016/j.semcancer.2015.02.006
PMID:25892662

14. Zhan T, Rindtorff N, Boutros M. Wnt signaling in cancer. Oncogene. 2017; 36:1461–73.
https://doi.org/10.1038/onc.2016.304
PMID:27617575

15. Aster JC, Pear WS, Blacklow SC. The varied roles of notch in cancer. Annu Rev Pathol. 2017; 12:245–75.
https://doi.org/10.1146/annurev-pathol-052016-100127 PMID:27959635

16. Calses PC, Crawford JJ, Lill JR, Dey A. Hippo pathway in cancer: aberrant regulation and therapeutic opportunities. Trends Cancer. 2019; 5:297–307.
https://doi.org/10.1016/j.trecan.2019.04.001
PMID:31174842

17. VanderVorst K, Hatakeyama J, Berg A, Lee H, Carraway KL 3rd. Cellular and molecular mechanisms underlying planar cell polarity pathway contributions to cancer Malignancy. Semin Cell Dev Biol. 2018; 81:78–87.
https://doi.org/10.1016/j.semcdb.2017.09.026
PMID:29107170

18. Daulat AM, Bertucci F, Audebert S, Sergé A, Finetti P, Josselin E, Castellano R, Birnbaum D, Angers S, Borg JP. PRICKLE1 contributes to cancer cell dissemination through its interaction with mTORC2. Dev Cell. 2016; 37:311–25.
https://doi.org/10.1016/j.devcel.2016.04.011
PMID:27184734

19. Zhang L, Luga V, Armitage SK, Musiol M, Won A, Yip CM, Plotnikov SV, Wrana JL. A lateral signalling pathway coordinates shape volatility during cell migration. Nat Commun. 2016; 7:11714.
https://doi.org/10.1038/ncomms11714
PMID:27226243

20. Dyberg C, Papachristou P, Haug BH, Lagercrantz H, Kogner P, Ringstedt T, Wickström M, Johnsen JI. Planar cell polarity gene expression correlates with tumor cell viability and prognostic outcome in neuroblastoma. BMC Cancer. 2016; 16:259.
https://doi.org/10.1186/s12885-016-2293-2
PMID:27036398

21. Gray RS, Abitua PB, Wlodarczyk BJ, Szabo-Rogers HL, Blanchard O, Lee I, Weiss GS, Liu KJ, Marcotte EM, Wallingford JB, Finnell RH. The planar cell polarity effector Fuz is essential for targeted membrane trafficking, ciliogenesis and mouse embryonic development. Nat Cell Biol. 2009; 11:1225–32.
https://doi.org/10.1038/ncb1966 PMID:19767740

22. Zhang Z, Wlodarczyk BJ, Niederreither K, Venugopalan S, Florez S, Finnell RH, Amendt BA. Fuz regulates craniofacial development through tissue specific responses to signaling factors. PLoS One. 2011; 6:e24608.
https://doi.org/10.1371/journal.pone.0024608
PMID:21935430

23. Chen ZS, Li L, Peng S, Chen FM, Zhang Q, An Y, Lin X, Li W, Koon AC, Chan TF, Lau KF, Ngo JC, Wong WT, et al. Planar cell polarity gene Fuz triggers apoptosis in

neurodegenerative disease models. EMBO Rep. 2018; 19:e45409.
https://doi.org/10.15252/embr.201745409
PMID:30026307

24. Hao X, Luo H, Krawczyk M, Wei W, Wang W, Wang J, Flagg K, Hou J, Zhang H, Yi S, Jafari M, Lin D, Chung C, et al. DNA methylation markers for diagnosis and prognosis of common cancers. Proc Natl Acad Sci USA. 2017; 114:7414–19.
https://doi.org/10.1073/pnas.1703577114
PMID:28652331

25. Greenberg MV, Bourc'his D. The diverse roles of DNA methylation in mammalian development and disease. Nat Rev Mol Cell Biol. 2019; 20:590–607.
https://doi.org/10.1038/s41580-019-0159-6
PMID:31399642

26. Chakravarthi BV, Nepal S, Varambally S. Genomic and epigenomic alterations in cancer. Am J Pathol. 2016; 186:1724–35.
https://doi.org/10.1016/j.ajpath.2016.02.023
PMID:27338107

27. Li LC, Dahiya R. MethPrimer: designing primers for methylation PCRs. Bioinformatics. 2002; 18:1427–31.
https://doi.org/10.1093/bioinformatics/18.11.1427
PMID:12424112

28. Yang N, Leung EL, Liu C, Li L, Eguether T, Jun Yao XJ, Jones EC, Norris DA, Liu A, Clark RA, Roop DR, Pazour GJ, Shroyer KR, Chen J. INTU is essential for oncogenic Hh signaling through regulating primary cilia formation in basal cell carcinoma. Oncogene. 2017; 36:4997–5005.
https://doi.org/10.1038/onc.2017.117 PMID:28459465

29. He Z, Wu X, Ma S, Zhang C, Zhang Z, Wang S, Yu S, Wang Q. Next-generation sequencing identified a novel WDPCP-ALK fusion sensitive to crizotinib in lung adenocarcinoma. Clin Lung Cancer. 2019; 20:e548–51.
https://doi.org/10.1016/j.cllc.2019.06.001
PMID:31281052

30. Natanzon Y, Earp M, Cunningham JM, Kalli KR, Wang C, Armasu SM, Larson MC, Bowtell DD, Garsed DW, Fridley BL, Winham SJ, Goode EL. Genomic analysis using regularized regression in high-grade serous ovarian cancer. Cancer Inform. 2018; 17:1176935118755341.
https://doi.org/10.1177/1176935118755341
PMID:29434467

31. Gerondopoulos A, Strutt H, Stevenson NL, Sobajima T, Levine TP, Stephens DJ, Strutt D, Barr FA. Planar cell polarity effector proteins inturned and fuzzy form a Rab23 GEF complex. Curr Biol. 2019; 29:3323–30.e8.
https://doi.org/10.1016/j.cub.2019.07.090
PMID:31564489

32. Tan WL, Jain A, Takano A, Newell EW, Iyer NG, Lim WT, Tan EH, Zhai W, Hillmer AM, Tam WL, Tan DS. Novel therapeutic targets on the horizon for lung cancer. Lancet Oncol. 2016; 17:e347–62.
https://doi.org/10.1016/S1470-2045(16)30123-1
PMID:27511159

33. Johnson DE, Burtness B, Leemans CR, Lui VW, Bauman JE, Grandis JR. Head and neck squamous cell carcinoma. Nat Rev Dis Primers. 2020; 6:92.
https://doi.org/10.1038/s41572-020-00224-3
PMID:33243986

34. Sanchez-Vega F, Mina M, Armenia J, Chatila WK, Luna A, La KC, Dimitriadoy S, Liu DL, Kantheti HS, Saghafinia S, Chakravarty D, Daian F, Gao Q, et al, and Cancer Genome Atlas Research Network. Oncogenic signaling pathways in the cancer genome atlas. Cell. 2018; 173:321–37.e10.
https://doi.org/10.1016/j.cell.2018.03.035
PMID:29625050

35. Dominguez-Brauer C, Thu KL, Mason JM, Blaser H, Bray MR, Mak TW. Targeting mitosis in cancer: emerging strategies. Mol Cell. 2015; 60:524–36.
https://doi.org/10.1016/j.molcel.2015.11.006
PMID:26590712

36. Kastan MB, Bartek J. Cell-cycle checkpoints and cancer. Nature. 2004; 432:316–23.
https://doi.org/10.1038/nature03097 PMID:15549093

37. Beckerman R, Prives C. Transcriptional regulation by p53. Cold Spring Harb Perspect Biol. 2010; 2:a000935.
https://doi.org/10.1101/cshperspect.a000935
PMID:20679336

38. Diab A, Gem H, Swanger J, Kim HY, Smith K, Zou G, Raju S, Kao M, Fitzgibbon M, Loeb KR, Rodriguez CP, Méndez E, Galloway DA, et al. FOXM1 drives HPV+ HNSCC sensitivity to WEE1 inhibition. Proc Natl Acad Sci USA. 2020; 117:28287–96.
https://doi.org/10.1073/pnas.2013921117
PMID:33093209

39. van Harten AM, Buijze M, van der Mast R, Rooimans MA, Martens-de Kemp SR, Bachas C, Brink A, Stigter-van Walsum M, Wolthuis RM, Brakenhoff RH. Targeting the cell cycle in head and neck cancer by Chk1 inhibition: a novel concept of bimodal cell death. Oncogenesis. 2019; 8:38.
https://doi.org/10.1038/s41389-019-0147-x
PMID:31209198

40. Zhou G, Liu Z, Myers JN. TP53 mutations in head and neck squamous cell carcinoma and their impact on disease progression and treatment response. J Cell Biochem. 2016; 117:2682–92.
https://doi.org/10.1002/jcb.25592 PMID:27166782

41. Verduci L, Ferraiuolo M, Sacconi A, Ganci F, Vitale J, Colombo T, Paci P, Strano S, Macino G, Rajewsky N, Blandino G. The oncogenic role of circPVT1 in head and neck squamous cell carcinoma is mediated through the mutant p53/YAP/TEAD transcription-competent complex. Genome Biol. 2017; 18:237.
https://doi.org/10.1186/s13059-017-1368-y
PMID:29262850

42. Ganci F, Pulito C, Valsoni S, Sacconi A, Turco C, Vahabi M, Manciocco V, Mazza EM, Meens J, Karamboulas C, Nichols AC, Covello R, Pellini R, et al. PI3K inhibitors curtail MYC-dependent mutant p53 gain-of-function in head and neck squamous cell carcinoma. Clin Cancer Res. 2020; 26:2956–71.
https://doi.org/10.1158/1078-0432.CCR-19-2485
PMID:31969334

43. Caponio VC, Troiano G, Adipietro I, Zhurakivska K, Arena C, Mangieri D, Mascitti M, Cirillo N, Lo Muzio L. Computational analysis of TP53 mutational landscape unveils key prognostic signatures and distinct pathobiological pathways in head and neck squamous cell cancer. Br J Cancer. 2020; 123:1302–14.
https://doi.org/10.1038/s41416-020-0984-6
PMID:32684626

44. Fukui T, Shaykhiev R, Agosto-Perez F, Mezey JG, Downey RJ, Travis WD, Crystal RG. Lung adenocarcinoma subtypes based on expression of human airway basal cell genes. Eur Respir J. 2013; 42:1332–44.
https://doi.org/10.1183/09031936.00144012
PMID:23645403

45. Auerbach O, Stout AP. Histopathological aspects of occult cancer of the lung. Ann N Y Acad Sci. 1964; 114:803–10.
https://doi.org/10.1111/j.1749-6632.1964.tb40999.x
PMID:5220116

46. Bao Z, Huang WJ. Thioridazine promotes primary ciliogenesis in lung cancer cells through enhancing cell autophagy. Int J Clin Exp Med. 2017; 10:13960–69.

47. Seo JH, Zilber Y, Babayeva S, Liu J, Kyriakopoulos P, De Marco P, Merello E, Capra V, Gros P, Torban E. Mutations in the planar cell polarity gene, fuzzy, are associated with neural tube defects in humans. Hum Mol Genet. 2011; 20:4324–33.
https://doi.org/10.1093/hmg/ddr359 PMID:21840926

48. Daste F, Galli T, Tareste D. Structure and function of longin SNAREs. J Cell Sci. 2015; 128:4263–72.
https://doi.org/10.1242/jcs.178574 PMID:26567219

49. De Franceschi N, Wild K, Schlacht A, Dacks JB, Sinning I, Filippini F. Longin and GAF domains: structural evolution and adaptation to the subcellular trafficking machinery. Traffic. 2014; 15:104–21.

https://doi.org/10.1111/tra.12124
PMID:24107188

50. Kandachar V, Tam BM, Moritz OL, Deretic D. An interaction network between the SNARE VAMP7 and rab GTPases within a ciliary membrane-targeting complex. J Cell Sci. 2018; 131:jcs222034.
https://doi.org/10.1242/jcs.222034 PMID:30404838

51. Nagy Á, Lánczky A, Menyhárt O, Győrffy B. Validation of miRNA prognostic power in hepatocellular carcinoma using expression data of independent datasets. Sci Rep. 2018; 8:9227.
https://doi.org/10.1038/s41598-018-27521-y
PMID:29907753

52. Grossman RL, Heath AP, Ferretti V, Varmus HE, Lowy DR, Kibbe WA, Staudt LM. Toward a shared vision for cancer genomic data. N Engl J Med. 2016; 375:1109–12.
https://doi.org/10.1056/NEJMp1607591
PMID:27653561

53. Anders S, Pyl PT, Huber W. HTSeq—a python framework to work with high-throughput sequencing data. Bioinformatics. 2015; 31:166–69.
https://doi.org/10.1093/bioinformatics/btu638
PMID:25260700

54. Love MI, Huber W, Anders S. Moderated estimation of fold change and dispersion for RNA-seq data with DESeq2. Genome Biol. 2014; 15:550.
https://doi.org/10.1186/s13059-014-0550-8
PMID:25516281

55. Subramanian A, Tamayo P, Mootha VK, Mukherjee S, Ebert BL, Gillette MA, Paulovich A, Pomeroy SL, Golub TR, Lander ES, Mesirov JP. Gene set enrichment analysis: a knowledge-based approach for interpreting genome-wide expression profiles. Proc Natl Acad Sci USA. 2005; 102:15545–50.
https://doi.org/10.1073/pnas.0506580102
PMID:16199517

56. Szklarczyk D, Gable AL, Lyon D, Junge A, Wyder S, Huerta-Cepas J, Simonovic M, Doncheva NT, Morris JH, Bork P, Jensen LJ, Mering CV. STRING v11: protein-protein association networks with increased coverage, supporting functional discovery in genome-wide experimental datasets. Nucleic Acids Res. 2019; 47:D607–13.
https://doi.org/10.1093/nar/gky1131 PMID:30476243

57. Huang da W, Sherman BT, Lempicki RA. Systematic and integrative analysis of large gene lists using DAVID bioinformatics resources. Nat Protoc. 2009; 4:44–57.
https://doi.org/10.1038/nprot.2008.211
PMID:19131956

58. Gao J, Aksoy BA, Dogrusoz U, Dresdner G, Gross B, Sumer SO, Sun Y, Jacobsen A, Sinha R, Larsson E, Cerami E, Sander C, Schultz N. Integrative analysis of

complex cancer genomics and clinical profiles using the cBioPortal. Sci Signal. 2013; 6:pl1.
https://doi.org/10.1126/scisignal.2004088
PMID:23550210

59. Li L, Xu J, Qiu G, Ying J, Du Z, Xiang T, Wong KY, Srivastava G, Zhu XF, Mok TS, Chan AT, Chan FK, Ambinder RF, Tao Q. Epigenomic characterization of a p53-regulated 3p22.2 tumor suppressor that inhibits STAT3 phosphorylation via protein docking and is frequently methylated in esophageal and other carcinomas. Theranostics. 2018; 8:61–77.
https://doi.org/10.7150/thno.20893
PMID:29290793
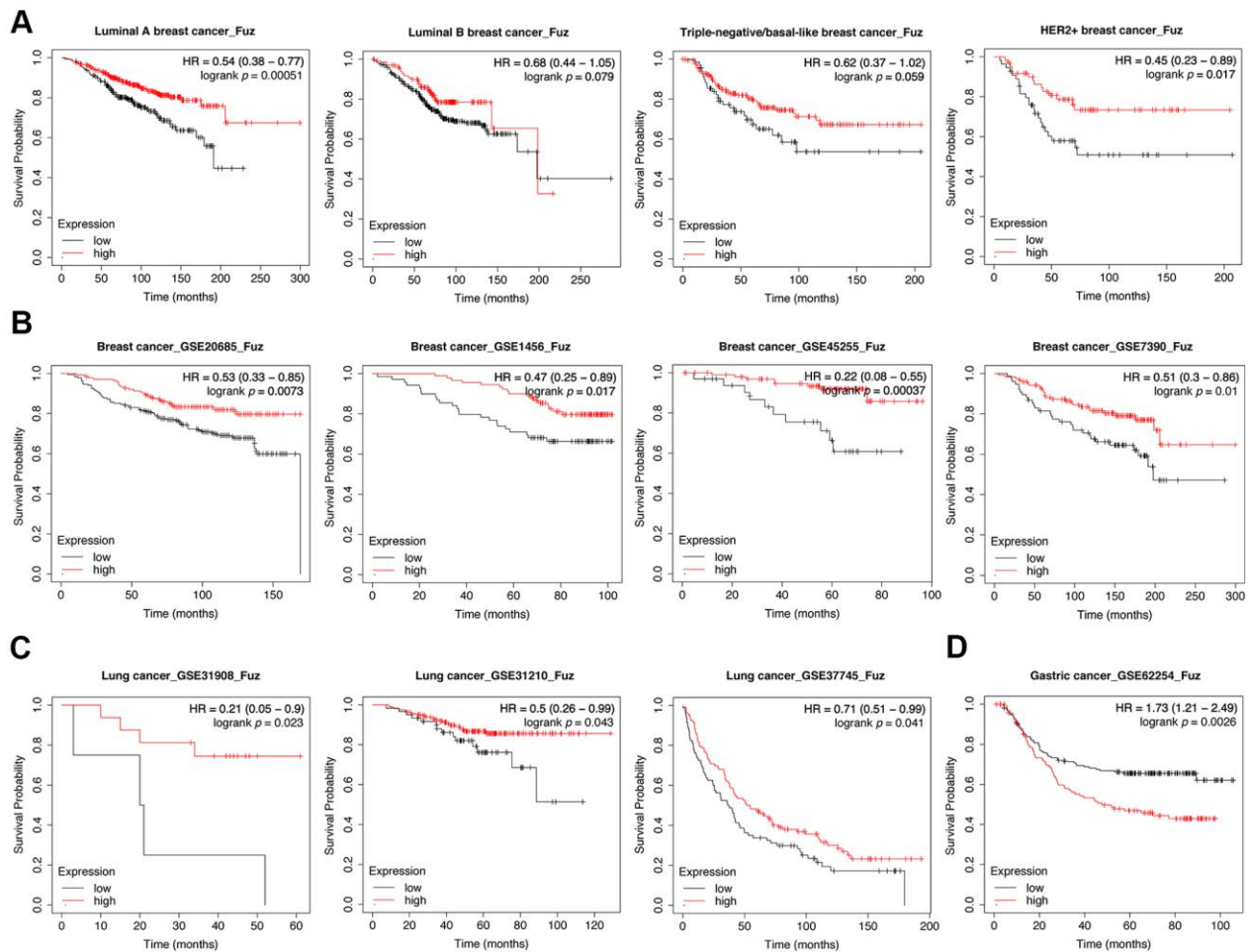
Supplementary Figure 1. Evaluation of the prognostic significance of *Fuz* mRNA expression in different subtypes of breast cancer and different cancer types. (**A**) Low level of *Fuz* expression correlated with poor prognosis in luminal A and HER2+ breast cancer patients, whilst no significant correlation was found in luminal B and triple-negative/basal-like breast cancer patients. (**B**–**D**) The correlation between low *Fuz* expression and poor prognosis of breast cancer (**B**), lung cancer (**C**) and gastric cancer (**D**) patients was further validated using additional GEO datasets.
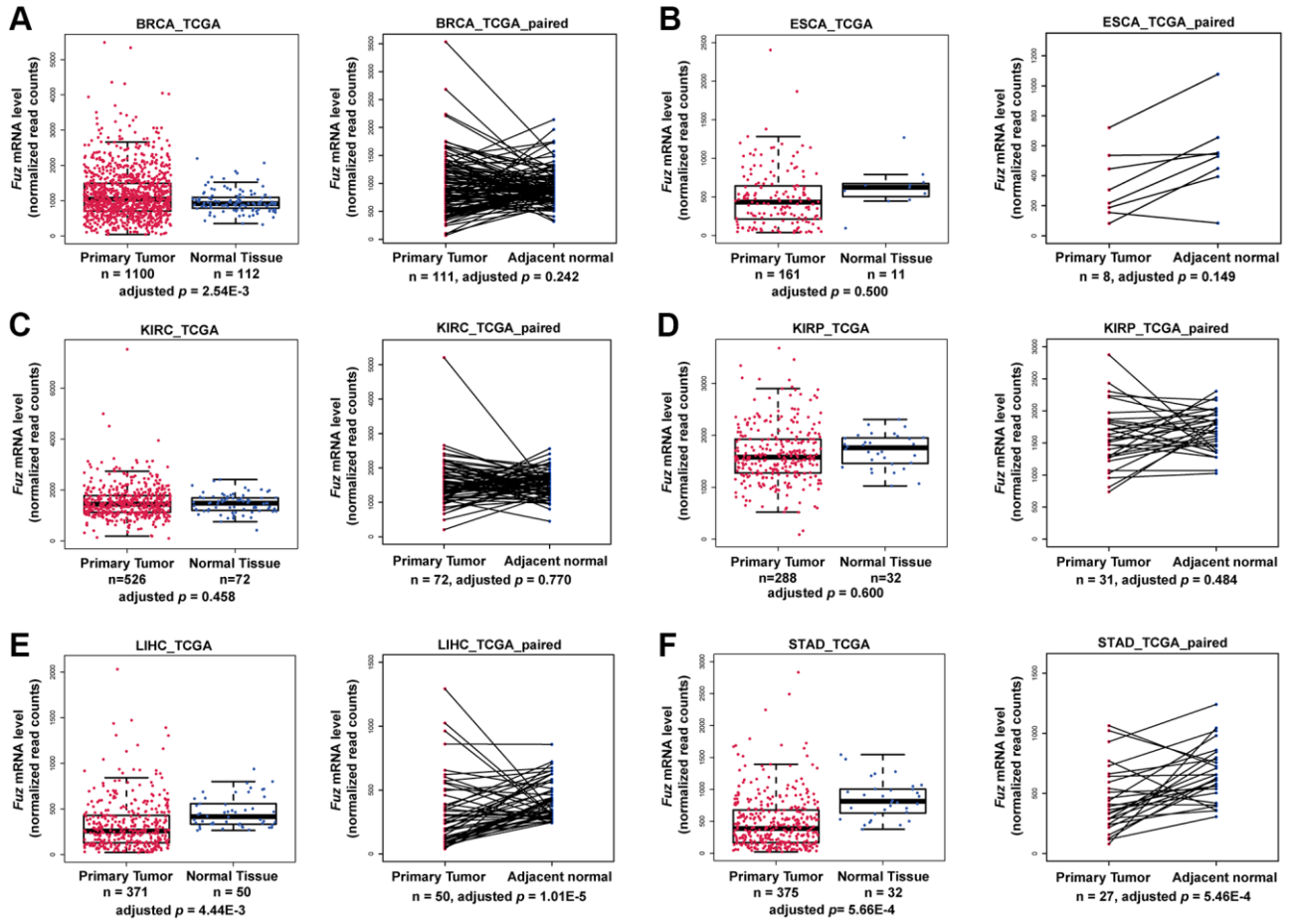
Supplementary Figure 2. Investigation of Fuz transcript level in different types of cancer. (**A**–**F**) Significant changes in Fuz mRNA level was found in tumor tissues from BRCA (**A**), LIHC (**E**) and STAD (**F**) patients. Downregulation of Fuz was further found in paired samples from LIHC (**E**) and STAD (**F**) patients. No significant changes in Fuz mRNA level were identified in tumor tissues from ESCA (**B**), KIRC (**C**) and KIRP (**D**) patients.
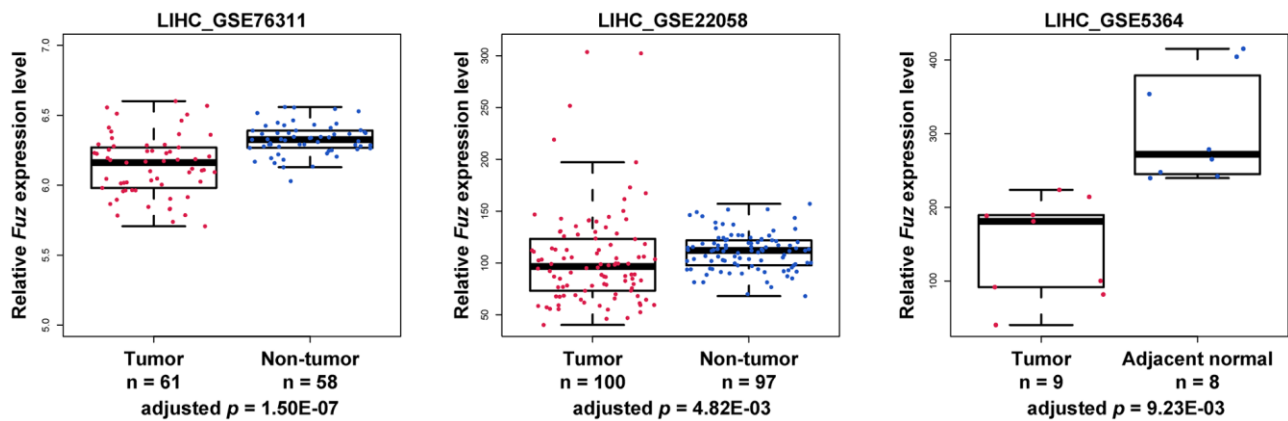

Supplementary Figure 3. Downregulation of Fuz expression level was further validated in additional LIHC datasets of GSE76311, GSE22058 and GSE5364.

Survival analysis for ESCA patients

$p = 0.044$

⊤ *Fuz* > 295.4986 (High expression group; n = 99)

+ *Fuz* < 295.4986 (Low expression group; n = 62)
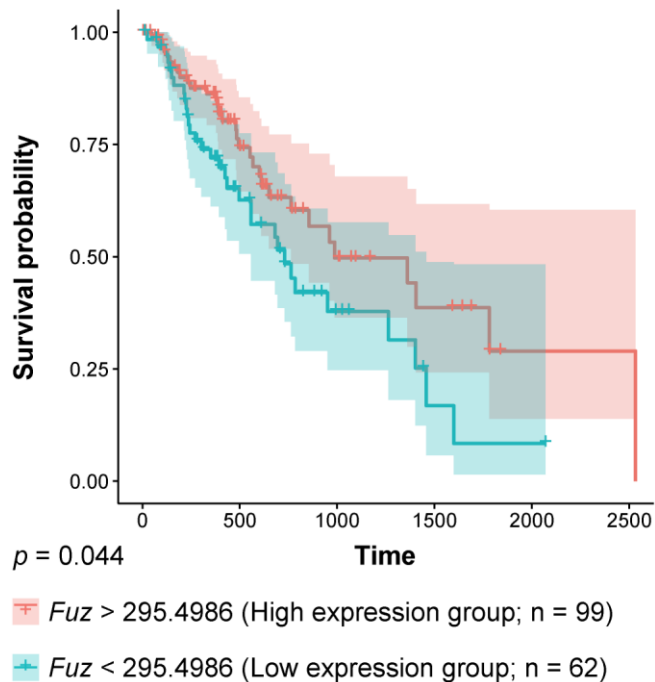
Supplementary Figure 4. The ESCA primary tumor tissues were divided into high *Fuz* expression and low *Fuz* expression groups based on the patient survival probabilities. Low *Fuz* expression associated with poor survival probabilities from ESCA patients.
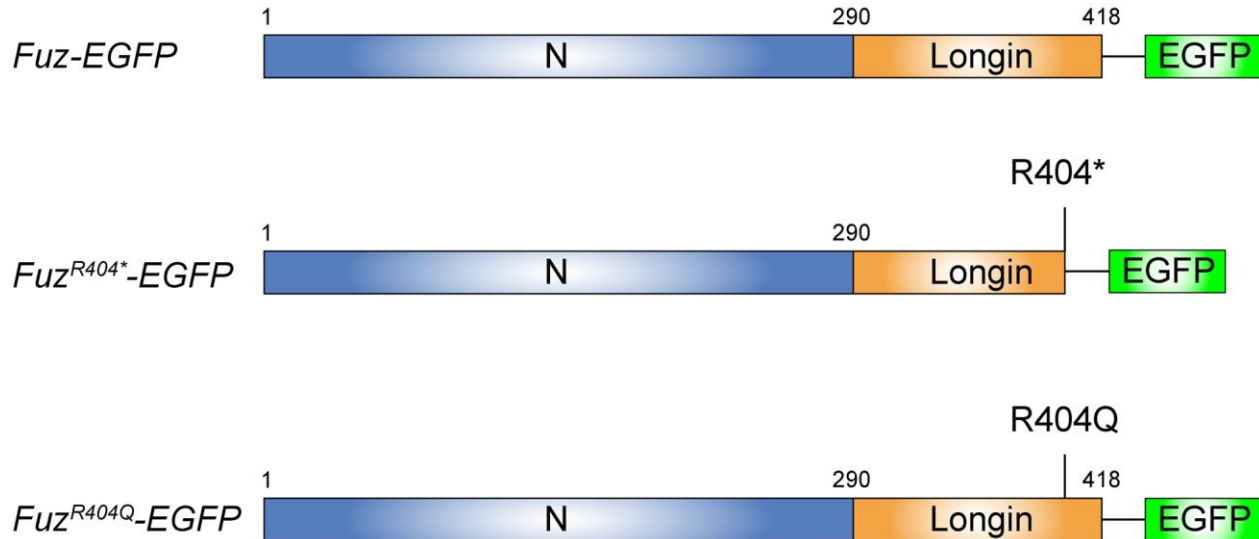
Supplementary Figure 5. Wildtype and mutant Fuz constructs used in the functional experiments. The location of R404* and R404Q mutations are shown.

Supplementary Tables

Supplementary Table 1. Multivariate analysis of correlation of different disease parameters in BRCA, ESCA, HNSC, KIRC, KIRP, LIHC, LUAD or STAD patients.

Parameter	Multivariate analysis_BRCA			Multivariate analysis_ESCA		
	HR	95% Cl	*p* value	HR	95% Cl	*p* value
Gender	0.9537	0.1292 - 7.042	0.9630	1.247	0.0927 - 16.766	0.8679
Race	0.893	0.6298 - 1.266	0.5250	0.725	0.3132 - 1.678	0.45264
Ethnicity	5.8278	0.8107 - 41.895	0.0799	1.469	0.1216 - 17.765	0.76212
Primary diagnosis	0.7095	0.5378 - 0.936	0.0152	1.904	0.6730 - 5.384	0.22494
Tumor stage	1.2114	1.1428 - 1.284	1.10E-10	1.525	1.1233 - 2.071	0.00682
Age at diagnosis	1.0001	1.0001 - 1.000	1.28E-08	1.000	0.9999 - 1.000	0.40249
Fuz level	0.9996	0.9993 – 1.000	0.0106	0.998	0.9957 - 1.000	0.09167

Parameter	Multivariate analysis_HNSC			Multivariate analysis_KIRC		
	HR	95% Cl	*p* value	HR	95% Cl	*p* value
Gender	0.8247	0.5842 - 1.164	0.27342	0.9170	0.6353 - 1.324	0.64357
Race	0.8430	0.6128 - 1.160	0.29424	0.9811	0.5549 - 1.735	0.94774
Ethnicity	0.9505	0.4698 - 1.923	0.88771	4.8638	1.5412 - 15.350	0.00698
Primary diagnosis	0.9786	0.9571 - 1.001	0.05591	N/A	N/A	N/A
Tumor stage	1.5944	1.3186 - 1.928	1.48E-06	1.8836	1.6176 - 2.193	3.56E-16
Age at diagnosis	1.0001	1.0000 - 1.000	0.00296	1.0001	1.0000 - 1.000	0.00224
Fuz level	0.9995	0.9989 - 1.000	0.10457	1.0000	0.9997 - 1.000	0.93238

Parameter	Multivariate analysis_KIRP			Multivariate analysis_LIHC		
	HR	95% Cl	*p* value	HR	95% Cl	*p* value
Gender	0.798	0.3419 - 1.863	0.60189	0.8888	0.5772 - 1.369	0.593
Race	0.805	0.3225 - 2.010	0.64221	0.9669	0.7706 - 1.213	0.771
Ethnicity	2.1369	0.2799 - 16.317	0.46407	1.2104	0.4700 - 3.117	0.692
Primary diagnosis	N/A	N/A	N/A	N/A	N/A	N/A
Tumor stage	2.9383	2.0429 - 4.226	6.18E-09	1.2998	1.1749 - 1.438	3.64E-07
Age at diagnosis	1.0001	1.0000 - 1.000	0.06171	1.0000	1.0000 - 1.000	0.369
Fuz level	0.9988	0.9981 – 1.000	0.00241	1.0001	0.9994 - 1.001	0.825

Parameter	Multivariate analysis_LUAD			Multivariate analysis_STAD		
	HR	95% Cl	*p* value	HR	95% Cl	*p* value
Gender	0.9682	0.6656 - 1.408	0.866	1.071	0.6869 - 1.670	0.76191
Race	1.2936	0.8047 - 2.080	0.288	1.052	0.8713 - 1.270	0.59922
Ethnicity	1.1651	0.2779 - 4.885	0.834	N/A	N/A	N/A
Primary diagnosis	0.9688	0.8138 - 1.153	0.721	9.533	0.7760 - 1.171	0.64897
Tumor stage	1.2151	1.1197 - 1.319	3.04E-06	1.181	1.0738 - 1.300	6.24E-04
Age at diagnosis	1.0000	1.0000 - 1.000	0.414	1.000	1.0000 - 1.000	0.02021
Fuz level	1.0001	0.9996 - 1.001	0.593	1.001	1.0002 - 1.001	0.00257

Supplementary Table 2. The detailed number of cases with *Fuz* genomic alterations in different types of cancer.

Cancer types	Total cases	Altered cases				
		Mutation	Amplification	Deep deletion	Multiple alterations	Fusion
Endometrial Carcinoma	586	14 (2.39%)	8 (1.37%)	1 (0.17%)	0	0
Adrenocortical Carcinoma	91	0	3 (3.3%)	0	0	0
Cholangiocarcinoma	36	1 (2.78%)	0	0	0	0
Bladder Urothelial Carcinoma	411	5 (1.22%)	5 (1.22%)	0	0	0
Mature B-Cell Neoplasms	48	0	0	1 (2.08%)	0	0
Pancreatic Adenocarcinoma	184	1 (0.54%)	2 (1.09%)	0	0	0
Diffuse Glioma	513	0	0	8 (1.56%)	0	0
Invasive Breast Carcinoma	1084	0	13 (1.2%)	1 (0.09%)	1 (0.09%)	0
Cervical Squamous Cell Carcinoma	251	1 (0.4%)	2 (0.8%)	0	0	0
Esophagogastric Adenocarcinoma	514	3 (0.58%)	3 (0.58%)	0	0	0
Non-Seminomatous Germ Cell Tumor	86	1 (1.16%)	0	0	0	0
Colorectal Adenocarcinoma	594	5 (0.84%)	0	0	0	0
Thymic Epithelial Tumor	123	0	0	1 (0.81%)	0	0
Prostate Adenocarcinoma	494	1 (0.2%)	1 (0.2%)	2 (0.4%)	0	0
Sarcoma	255	1 (0.39%)	0	1 (0.39%)	0	0
Melanoma	444	3 (0.68%)	0	0	0	0
Non-Small Cell Lung Cancer	1053	4 (0.38%)	2 (0.19%)	0	0	0
Ovarian Epithelial Tumor	584	1 (0.17%)	2 (0.34%)	0	0	0
Head and Neck Squamous Cell Carcinoma	523	1 (0.19%)	1 (0.19%)	0	0	0
Glioblastoma	592	0	1 (0.17%)	0	0	1 (0.17%)
Hepatocellular Carcinoma	369	0	1 (0.27%)	0	0	0
Renal Clear Cell Carcinoma	511	0	0	1 (0.2%)	0	0

Supplementary Files

Please browse Full Text version to see the data of Supplementary Files 1, 2.

Supplementary File 1. The gene ranks used for GSEA analysis.

Supplementary File 2. The alterations of *Fuz* promoter methylation in different types of cancer.